Studies on a Stellarator Reactor of the Helias Type: The Modular Coil System

Ewald Harmeyer, Johann Kißlinger,
Fritz Rau, Horst Wobig

IPP 2/316 February 1993

MAX-PLANCK-INSTITUT FÜR PLASMAPHYSIK

8046 GARCHING BEI MÜNCHEN

MAX-PLANCK-INSTITUT FÜR PLASMAPHYSIK

GARCHING BEI MÜNCHEN

Studies on a Stellarator Reactor of the Helias Type: The Modular Coil System

Ewald Harmeyer, Johann Kißlinger,
Fritz Rau, Horst Wobig

IPP 2/316 February 1993

Die nachstehende Arbeit wurde im Rahmen des Vertrages zwischen dem Max-Planck-Institut für Plasmaphysik und der Europäischen Atomgemeinschaft über die Zusammenarbeit auf dem Gebiete der Plasmaphysik durchgeführt.

Table of Contents

Abstract

Helias Stellarator Reactors (HSR) are considered, focussing on the superconducting modular coil system which generates the magnetic field, aiming to clarify critical issues of such systems. The development of the coil system is presented and the properties of the vacuum magnetic field are discussed. Electromagnetic forces and the resulting mechanical stresses and strains inside the coils and the surrounding structure are calculated. Parameter studies are made varying the major radius R_0 between 18 m and 24 m in order to investigate the engineering parameters for the superconducting coil system. The total mass and the fusion power output of HSR are compared with values evaluated for tokamak reactors.

The present study is part of further studies on Stellarator reactors of the Helias type. Other parts will consider the plasma parameters, the divertor, the maintenance concept, and the aspects of environmental impact and inherent safety.

1. Introduction

The Stellarator is a concept for magnetic confinement of toroidal plasmas where the plasma equilibrium is maintained by currents located exclusively outside the plasma region. The magnetic field is generated by a single set of modular non-planar coils. A reactor of this type can be operated in steady state. There are no disruptive instabilities and the level of recirculating power is low. The ratio between surface and volume of the machine is favourable, consequently the neutron wall load is moderate.

In continuation of the Advanced Stellarator line at IPP Garching a Helias [1] configuration is employed in the future experiment Wendelstein 7-X [2] . The specific features of Helias configurations are the reduction of the Pfirsch-Schlüter currents to a small level ($J_{||} < J_{\perp}$) which leads to a small Shafranov shift and to a small neoclassical transport. MHD-stability limits are expected at $\bar{\beta} = 4-5\%$ which is sufficient for reactor performance. Bootstrap currents in Helias configurations can be kept at a low level so that the magnetic field is not affected by them.

The Helias reactor (HSR) is a scaled-up version of the magnetic field configuration envisaged for the Wendelstein 7-X experiment [3] [4]. However, in contrast to Wendelstein 7-X, a larger magnetic mirror ($\delta B/B \approx 10\%$) on the magnetic axis has been introduced to provide an improved confinement of high energy α-particles. Two versions, HSR 5-8 and HSR 5-10, are treated in this report. In HSR 5-8 this mirror field is achieved [5] by energizing the modular coils with different currents as it is also intended in the Wendelstein 7-X experiment. In version HSR 5-10 this mirror effect is provided [6] by the geometric arrangement of the modular coils alone, with equal currents in all coils.

Version HSR 5-10 provides also more space for divertor structures than HSR 5-8, which unavoidably leads to a larger size of the coils by roughly 10%. In both systems however, the magnetic field topology inside the separatrix is nearly the same so that no differences in plasma performance have to be expected.

In contrast to a previous study of an Advanced Stellarator Reactor, called the ASRA6C study, the Helias concept offers the chance to obtain a self-consistent reactor concept where

---

1) Nührenberg, J., Zille, R., Stable Stellarators with Medium β and Aspect Ratio, Physical Letters 114A, 129 (1986).

2) Grieger, G., et al., Physics and Engineering Studies for Wendelstein 7-X, Proceedings of the 13th Int. Conf. on Plasma Physics and Contr. Nuclear Fusion Research, Washington, DC, 1990, IAEA-CN-53/G-1-6, Vienna 1991, Vol.III, 525.

3) Grieger, G., Modular Stellarator Reactors and Plans for WENDELSTEIN 7-X, Fusion Technology, Vol.21, No.3, (1992), 1767.

4) Beidler, C., Grieger, G., Harmeyer, E., et al., Reactor Studies on Advanced Stellarators, Proceedings of the 14th Int. Conf. on Plasma Physics and Contr. Nuclear Fusion Research, Würzburg, BRD, 1992, IAEA-CN-56/G-I-2, Vienna 1993, to be published.

5) Beidler, C., et al., Vacuum Fields and Parameter Range of a Modular Helias Configuration, Proceedings of the 16th European Conference on Contr. Fusion and Plasma Physics, Venezia, Italia, 1989, EPS, 13B, Part II, 595-598.

6) Kisslinger, J., et al., Magnetic Field and Coil Systems of the Modular Helias Configuration HS 5-10, Proceedings of the 16th Symposium on Fusion Technology, London, UK, 1990, Vol.2, 1520-1524.

plasma losses, stability limits and α-particle losses are not prohibitive to ignition, and 3 GW fusion power can be produced with reasonable reactor dimensions.

The present study gives an overview on characteristic data of the modular coil system of the reference cases HSR 5-8 and HSR 5-10. In section 2 the geometrical dimensions are considered, varying the major radius from $R_0 = 18$ m to $R_0 = 24$ m for HSR 5-8. Data of some tokamak rector studies are summarized for comparison. In section 3 the superconducting modular coil system is discussed in detail. Section 4 describes the properties of the vacuum magnetic field. The main part of the study is given in section 5. Here the results of the analysis of the electromagnetic forces at the coils and the mechanical stresses and strains inside the coils are presented. These results are achieved with the EFFI and SAP V(2) computer codes. A comparison with ITER and three recent tokamak reactors is given. Little attention has been given to the details of blanket and shield of HSR so far. In the context of the present study the geometrical dimensions are important only: A minimum distance occurs only on the inboard side of the plasma, at other places more room for a larger blanket and shield is available. The study is terminated by a summary and conclusions.

2. Geometrical dimensions

In scaling-up a Helias configuration to reactor dimensions several constraints exist which determine the size of the reactor:

- The magnetic field is a five-period Helias configuration. Similarity to Wendelstein 7-X should be as close as possible.
- The magnetic field on axis is limited to 5.0 T which allows to stay within the NbTi-technology.
- Sufficient space for shield, blanket and divertor systems has to be provided. This requires at least 1.2 m distance between first wall and coil winding pack and this sets a lower limit on the aspect ratio ($A \geq 12$).
- The coil system consists of one set of modular coils only. Extra coils like in Wendelstein 7-X are not necessary. The maintenance concept is based on removable modules consisting of 4 or 6 coils plus the underlying shield and blanket.
- The size is determined by the need for sufficient plasma confinement to reach ignition (the confinement time scales roughly with the plasma volume). An upper limit is given by the fusion power which should not exceed 3.5 GW in the stationary burn phase.

These conditions lead to typical reactor dimensions listed in Table I. The major radius is $R_0 = 20$ m with an average magnetic field $B_0 = 5$ T on axis at a stored magnetic energy of 74 GJ for HSR 5-8 and of 80 GJ for HSR 5-10. Fifty modular non-planar coils generate the magnetic field with a peak value of 10.6 T or 10.9 T, resp., at the winding pack of the coils. This allows the use of supercritical helium at 1.8 K for cooling the NbTi coils. The

coil aspect ratio is about 5; this value is in an optimum range [7] in view of the maximum field at the coils and the mechanical stresses inside the coils. Due to the five-fold symmetry of the magnetic field and the symmetry within one field period there are only 5 different coils, which appreciably facilitates the analysis. Because of the larger coil radius compared with HSR 5-8 the configuration HSR 5-10 needs more structural material, consequently the total weight increases by more than 20%.

Figure 2.1 shows the main components of a Helias rector in the upper part, and plasma and target plates in the lower part. The moderate helicity of the magnetic axis in the Helias configuration and the toroidally varying shape of the coil bores require a related helical geometry of the blanket and shield. A common cryostat surrounds the reactor. It is modulated for maintenance purpose. Figure 2.2 shows as example an overlay of the dimensions of HSR 5-8 and ITER.

Table I: Main data of the Helias reactors HSR 5-8 and HSR 5-10.

		HSR 5-8	HSR 5-10
Average major radius	[m]	20.	20.
Average coil radius	[m]	4.0	4.4
Number of coils		50	50
Induction on axis	[T]	5.0	5.0
Max. induction on coils	[T]	10.6	10.9
Total magnetic energy	[GJ]	74.	80.
Rotational transform on axis		0.84	0.86
Rotational transform on boundary		0.97	0.99
Average plasma radius	[m]	1.6	1.6
Plasma volume	[m^3]	10^3	10^3
Surface of first wall	[m^2]	2.2×10^3	2.3×10^3
Volume of blanket	[m^3]	700	1300
Mass of blanket ($\rho = 4$)	[t]	2.8×10^3	5.2×10^3
Volume of shield	[m^3]	1.7×10^3	1.8×10^3
Mass of shield ($\rho = 5$)	[t]	8.3×10^3	9.2×10^3
Total mass	[t]	$\approx 2.6 \times 10^4$	$\approx 3.2 \times 10^4$

[7] Harmeyer E., Untersuchung modularer Systeme aus nichtebenen Spulen für den Stellarator-Fusionsreaktor, Report IPP 2/298, Dezember 1988.

The dimensions of blanket and shield are taken from the ASRA6C study [8] modified by further input from various tokamak studies. For HSR 5-10 a blanket with 60 cm thickness and 90% coverage is assumed. This meets the condition that a minimum distance between coil winding pack and plasma of 1.2 m at the inboard side is required to provide sufficient space for blanket and shield needed for reactor operation during a lifetime of 30 years.

In order to investigate the dependence of the main system parameters from the geometrical dimensions studies are made varying the major radius from $R_0 = 18$ m to $R_0 = 24$ m, see Fig. 2.3. In Table II the main data of these different HSR 5-8 configurations are sumarized; in Table III the data of the HSR 5-10 configuration is compared with the data of some tokamak reactor studies.

Table II: Data of the coil system of four Helias reactors HSR 5-8 with a major radius R_0 between 18 m and 24 m, comprising 5 field periods and 10 coils within each, utilizing NbTi as superconductor at 1.8 K. The magnetic field on axis is 5 T.

Average major radius	[m]	18.	20.	22.	24.
Average coil radius	[m]	3.6	4.0	4.4	4.8
Max. induction on coils	[T]	10.8	10.6	10.4	10.3
Tot. inductance (one turn)	[mH]	1.18	1.30	1.42	1.54
Total magnetic energy	[GJ]	54.	74.	98.	126.
Winding pack					
Radial height	[m]	0.60	0.70	0.80	0.90
Lateral coil width	[m]	0.54	0.61	0.68	0.75
Max. tor. elongation	[m]	1.8	2.0	2.2	2.4
Volume	[m^3]	8.2	12.	16.9	22.8
Av. current density	[MA/m^2]	29.6	25.0	21.6	18.9
Av. coil current	[MA]	9.6	10.67	11.73	12.8
Av. force density	[MN/m^3]	80.7	67.6	58.3	51.1
Max. net force	[MN]	105.	129.	156.	185.
Total coil volume	[m^3]	411.	602.	845.	1142.
Total coil mass	[t]	2.6×10^3	3.8×10^3	5.3×10^3	7.1×10^3
Mass of structure	[t]	$\approx 6.2 \times 10^3$	$\approx 8.4 \times 10^3$	$\approx 11.2 \times 10^3$	$\approx 14.5 \times 10^3$
Virial stress	[MPa]	131.	122.	115.	110.
Total reactor mass	[t]	$\approx 20 \times 10^3$	$\approx 26 \times 10^3$	$\approx 33 \times 10^3$	$\approx 41 \times 10^3$

[8] Böhme, G., et al.: Studies of a Modular Advanced Stellarator Reactor ASRA6C, Report IPP 2/285, Mai 1987, also Report KfK 4268, and Report FPA-87-2.

The coil systems considered in Table II provide a mirror-field of about ±10% on plasma axis with maximum at the region of large axis curvature, i.e. near the 'corners' of the 'pentagonal shape' of Fig. 2.3. This feature is accomplished by increase of the coil current from coil 1 to coil 5 by ±5% of the average total amount listed in the table. The maximum field on coil surface amounts to $B_{max} = 10.6$ T for the system with $R_0 = 20$ m. If no additional mirror-field is applied a lower maximum field at the coils of $B_{max} = 10.2$ T is obtained, see Fig. 2.4. For the system with $R_0 = 24$ m it could even decrease below 10 T.

The total inductance of the coil systems varies between 1.18 mH and 1.54 mH for the four cases, if one turn coils are considered, and the related stored magnetic energy W_{mag} is between 54 GJ and 126 GJ. The virial stress σ_V characterizes the specific magnetic load of the coil system and is obtained by dividing the total stored magnetic energy by the total coil volume, $\sigma_V = W_{mag}/V_c$. In the four coil systems considered the value of the virial stress σ_V decreases from 131 MPa to 110 MPa. This means that the amount of structural steel necessary for mechanical support of the coil system increases slowlier than the system volume between $R_0 = 18$ m and $R_0 = 24$ m.

In Fig. 2.4 the system parameters of the maximum magnetic field B_{max}, the stored magnetic energy W_{mag}, the virial stress σ_V, and the current density j_c are shown versus the major radius R_0. When increasing the major radius at fixed magnetic field on axis, the coil radius is also increased, and the stored magnetic energy raises considerably, according to the increased torus volumen. On the other hand the maximum magnetic field, the virial stress, and the current density in the coils decrease when the major radius increases. This is due to the increasing cross-section of the coils.

As detailed in a further IPP report [9] on the plasma parameters of the Helias reactor the fusion power output of the four cases considered amounts to about 1.8 GW and 4 GW. For HSR with a radius of 20 m an electric power output of 1.1 GW is estimated. With a total mass of about 26000 t for the entire system this leads to a mass utilisation of approximately 40 kWe/t which is lower than values found in studies on Stellarator reactors of the ORNL-Group [10]; but it is an acceptable value in comparison to that of ITER [11] and recent tokamak reactors studies [12] [13]. The ARIES-I tokamak reactor [14] is out of the range of this data due to the fact that "ARIES-I is based upon extrapolations that in several cases extend beyond present engineering achievements". In Table III the main technical data of these configurations are summarized.

---

9) Wobig, H., et al., Studies on a Stellarator Reactor of the Helias Type: The Plasma Parameters, Report IPP 2/318, to be published.

10) Lyon, J.F., Painter, S.L., Assessment of Torsatrons as Reactors, Proceedings of the 34. Annual APS Meeting, Seattle, WA, 1992, Nov. 16-20.

11) ITER Conceptual Design Report, ITER Documentation Series No.18, IAEA, Vienna 1991.

12) Spears, W.R., A Prototype Commercial-Sized Reactor PCSR-E, Report NET No.67, EUR-FU/XII-80/86/67, Dec. 1986.

13) Concept Study of the Steady State Tokamak Reactor (SSTR), Report JAERI-M 91-081, June 1991.

14) Najmabadi, F., Conn, R.W., et al., The ARIES-I Tokamak Reactor Study, Proc. of the 16th Symposium on Fusion Technology, London, UK, (1990), Vol.2, 253, and, The ARIES-I Tokamak Reactor Study – Final Report, Report UCLA/PPG-1323, Vol.I and Vol.II, 1991.

Table III: Characteristic data of various reactor concepts:

In the table the main technical data of the Helias Reactor HSR 5-10 and the tokamak reactors ITER, PCSR-E, SSTR and ARIES-I are summarized. Version HSR 5-10 needs about 20% more structural material than HSR 5-8, however, compared with tokamak commercial reactors, the total mass values for HSR are in the same range.

	HSR 5-10	ITER	PCSR-E	SSTR	ARIES-I
Average major radius [m]	20.	6.0	9.3	7.0	6.8
Average plasma radius [m]	1.6	2.9	3.1	2.3	2.0
Plasma volume [m^3]	1000	1050	1750	760	540
TF-coils					
Average coil radius [m]	4.4	5.6	≈ 5.9	≈ 5.2	≈ 4.3
Average coil volume [m^3]	10.0	11.3	≈ 18.7	$\approx 30.$	≈ 20.9
Current density [MA/m^2]	31.8	35.1	35	20.8	31.2
Superconductor	NbTi	Nb_3Sn		$(NbTi)_3Sn$	Nb_3Sn
Temperature [K]	1.8	4.2		4.2	4.2
Total volume (winding pack)					
TF coils [m^3]	500	180	410	480	334
PF+OH coils [m^3]	0	≈ 320	≈ 600	≈ 230	≈ 220
Total number of coils	50	30	38	30	32
Mass of coil systems [kt]	15.8	9.8	17.4	13.7	4.8
Mass (blanket, shield) [kt]	≈ 14.4	≈ 8	≈ 7	≈ 7	≈ 3
Vacuum vessel [kt]	≈ 2.2	≈ 7.8	≈ 20	≈ 4.5	≈ 2.3
Total mass [kt]	≈ 32	≈ 25	≈ 44	≈ 26	≈ 10
Field on axis [T]	5.0	4.85	6.36	9.0	11.3
Max. field on coils [T]	10.9	11.4	11.3	16.5	21.
Magnetic energy (TF) [GJ]	80	42	115	137	126
Magnetic energy (Total) [GJ]	80	63	139	143	144
Max. net coil force [MN]	118	425		1378	
Fusion power [GW]	3.0	1.0	3.6	3.0	1.93

PCSR-E: European Tokamak Reactor Study (Report NET No.67, Dec. 1986).
SSTR: Steady State Tokamak Reactor (Report JAERI-M 91-081, June 1991).
ARIES-I: High-field Commercial Tokamak Reactor (Report UCLA/PPG 1223, 1991).

3. Development of the coil system

The coil system of Helias configurations is calculated after the plasma equilibrium has been specified. This procedure differs from the conventional approach, where the coil system is optimized and the plasma behaviour is investigated afterwards. The method used to define the coils of a Wendelstein 7-X configuration is decribed for an earlier data set in detail in [15]. The procedure consists of several steps:

- calculation of surface currents on a torus producing the desired magnetic field,
- construction of finite size coils,
- small modifications of the coils,
- computation of the vacuum field.

The first step uses a toroidal surface S_1 which represents the plama boundary of the given Helias configuration and a second surface S_2 (enclosing S_1 at a chosen radial distance) on which a surface current distribution is determined using the NESCOIL-code [16]. This current distribution is discretized into a finite number of current lines used as center filaments of the actual coils. The shape of S_2 and the number of Fourier components of the potential ϕ, from which the current lines are calculated, are optimized according to the following criteria:

- maximum distance between the plasma and surface S_2,
- maximum distance between two adjacent filaments,
- maximum radius of curvature of the filaments,
- quality of the resulting magnetic field with respect to the originally given field.

As a result of the optimization, the shape of the surface S_2 is similar to that of S_1. At the position where S_1 has a large indentation, considerable toroidal current components are necessary and consequently the distance between S_2 and the plasma boundary has there its minimum (about 1.5 m) which is bounded by the limits of density and curvature of the current lines. At most of the other positions (in the case of HSR 5-10 more than 90% of area of the first wall) the distance could be increased to more than 1.8 m, thereby reducing the modular magnetic ripple and providing space for in-vessel components; e.g. divertor target plates.

The rectangular cross-section of the coils is constructed by using the normal vector $\mathbf{n}$ on the surface S_2 as the direction of the coil height, and the direction perpendicular to $\mathbf{n}$ and the tangential vector of the central filament for the coil width. Locally, the edges of the coils may be curved too much; therefore a local smoothing has been applied to enhance the minimum radius of curvature. The chosen number of 10 coils per field period results from a compromise between small modular magnetic ripple and sufficient access to the plasma

---

[15] Beidler, C., et al., Physics and Engineering Design for WENDELSTEIN VII-X, Fusion Technology, Vol.17, No.1, (1990), 148ff.

[16] Merkel, P., Solution of Stellarator Boundary Value Problems with External Currents, Nuclear Fusion, Vol.27, No.1, (1987), 867ff.

and in-vessel components. Because of the 'Stellarator symmetry' the number of coil shapes is half the number of coils per period, e.g. there are 5 different coil shapes only.

4. Vacuum magnetic field

In calculating the magnetic field from the coil system the coils have been replaced by the central current filament followed by a computation of the field using Biot-Savart's law. Former studies have shown that in the plasma region this procedure is accurate enough and that a single central current filament yields the same field as a current distribution with e.g. 5 or 6 filaments which approximates a continuous current distribution.

The magnetic field of the reference case HSR 5-8 is scaled-up version of the Wendelstein 7-X configuration HS 5-8 [17] [18]. The rotational transform has been changed slightly ranging from $\iota = 0.86$ on axis to $\iota \approx 1$ on the boundary. This profile of ι has no major resonances ($\iota = 3/4, 5/6, 5/5$) in the plasma volume. In configuration HSR 5-8 the island at $\iota = 5/5$ on the plasma edge will not affect the plasma confinement; these islands can be utilized for divertor application. The plasma aspect ratio defined by the last closed magnetic surface is 12 which is a compromise between the plasma physics requirements of confinement and stability and sufficient space for blanket and shield. The magnetic well is negative ($\delta V'/V' \simeq 1\%$) which provides a threshold against ideal MHD instabilities.

The magnetic field of configuration HSR 5-10 is very similar to HSR 5-8. However, between plasma boundary and first wall more space is available for divertor components. In Fig. 4.1 Poincaré plots for HSR 5-10 of 2 toroidal planes, $\varphi = 0^o$ and $\varphi = 36^o$, are given. The figure clearly shows that the minimum distance between plasma and coils occurs on the inboard side of the plasma near the midplane only. In both configurations the magnetic mirror has been raised to $\delta B/2B \approx 0.1$ which leads to good confinement of high-energy α-particles within one field period. Details of this effect are discussed elsewhere [19].

5. Modular coil system

5.1. Coil winding pack

The winding pack of the superconducting modular coils for HSR is envisaged to be similar to that of the Wendelstein 7-X experiment, with some modifications, however. For this experiment a 'cable-in-conduit' conductor will be applied, using NbTi at 4 K with forced-flow cooling. This type of conductor was proposed during an industrial study of ABB [20] which had been ordered by IPP Garching in 1988. One result of the report was

[17] Beidler, C., et al., Vacuum Fields and Parameter Range of a Modular Helias Configuration, Proceedings of the 16th European Conference on Controlled Fusion and Plasma Physics, Venezia, Italia, 1989, EPS, 13B, Part II, 595-598.

[18] Kißlinger, J.,: Parameter Variations for W VII-X Vacuum Fields, Proceedings of the 3rd Ringberg Workshop on W VII-X, June 1989, Report IPP 2/302, 74ff.

[19] Lotz, W., et al., Collisionless α-Particle Confinement in Stellerators, Plasma Physics and Controlled Fusion, Vol.34, No.6, (1992), 1037.

[20] Maix, R.K., et.al., ABB-Schlussbericht: Machbarkeitsstudie über einen Supraleiter für Wendelstein VII-X, Asea Brown Bovery AG Zürich, Sept. 1989, S. 5-9.

that this type of cable is the best conductor solution in view of thermohydraulic behaviour, cryogenic stability, and feasibility of the coil winding pack. There is low risk of failure and a high degree of quality assurance. In the LCT-project [21] this type of cable, among others, has been tested with good results. Particularly for non-planar coils it seems to be the best conductor solution. Special winding requirements arise from the non-planar shape of the coils: during the winding procedure the conductor should be in a soft stage, while the final winding pack must be stiff in order to provide sufficient mechanical properties to manage the complex magnetic force distribution. This will be achieved using a cable jacket of soft annealed aluminium alloy [22] which can be hardened at moderate temperatures of about 160 °C during the resin impregnation of the insulation. The aluminium alloy jacket is applied on the conductor by coextrusion. Internal cooling is preferred because this allows the simultaneous wetting of the strands and the fabrication of a monolithic winding pack by vacuum impregnation. A pure copper matrix and strands with diameters of about half to one millimeter, cabled together, are sufficient to keep the AC losses low for frequencies up to 3 Hz [23] at small magnitudes. The nominal current of the Wendelstein 7-X conductor is 16 kA at cable dimensions of 16×16 mm^2 (insulated), as a compromise of coil feasibility and of the voltage expected during safety discharge.

The thermohydraulic and the electric behaviour of this conductor will be tested in the STAR test facility at KfK-Karlsruhe [24], and a full-size Demonstration Coil of the Wendelstein 7-X configuration will be constructed [25] in order to test the mechanical behaviour of the coil winding pack and the coil housing. The latter will be installed into the TOSKA facility at KfK-Karlsruhe, where the Euratom-LCT coil is used to generate the background magnetic field in order to raise the test field strength to a level used in Wendelstein 7-X.

For reactor applications it is believed that this type of conductor can be applied for HSR configurations also, using NbTi at 1.8 K with forced-flow cooling of superfluid helium, however. No particular thermal shielding between the winding pack and the coil housing is required, due to the low heat conduction across the outer winding pack insulation. The test of this particular important design principle is one of the aims in the future experiments with the Euratom-LCT coil of the TOSKA facility at KfK-Karlsruhe [26]. The HSR coil dimensions are roughly increased by about a factor of 3, compared with Wendelstein 7-X. With a total coil current of 10.6 MA the nominal current of the conductor should be between

---

21) Beards, D.S., et al., The IEA Large Coil Task, Fusion Engineering and Design, Vol.7, Nos.1+2, (1988).

22) Heller, R., Maurer, W., Sapper, J., et al., Superconductor Proposed for Wendelstein 7-X, Report KfK-Primärbericht No. 03.01.02 P 38A, Dec. 1990.

23) Heller, R., Jüngst, K.P., Maurer, W., Rieger, C., AC Losses of Wendelstein 7-X Coils, Report KfK-Primärbericht No. 31.03.08 P 01A, Oct. 1992.

24) Harmeyer, E., Schoenewolf, I., et al., Die Supraleiter-Testspule für W 7-X in der Anordnung STAR von KfK, Report IPP 2/315, Jan. 1992.

25) Harmeyer, E., et al., Force and Stress Calculations for a Non-Planar W VII-X Demonstration Coil, Proc. of the 16th Symp. on Fusion Technology, London, UK, (1990), Vol.2, 1515.

26) Grünhagen, A., et al., Preparations of the TOSKA Facility at KfK for Testing of NET Model Coils, Proceedings of the 16th Symposium on Fusion Technology, London, UK, (1990), Vol.2, 1692.

30 and 40 kA. The associated conductor dimensions can be increased because the minimum radius of coil curvature is about 60 cm for the reactor coils. Although a detailed design of the conductor for HSR is not yet available the extrapolation of the Wendelstein 7-X conductor is credible, and will be substantiated when the test of the Euratom-LCT coil at 1.8 K has been made.

5.2. Electromagnetic forces

The magnetic forces on the modular coils determine the geometry of the support system and cause the mechanical stresses and strains, which are to be kept below engineering limits. The magnetic field inside the coils and the magnetic forces are calculated using the EFFI code [27]. A complex magnetic field distribution exists inside the coils, which leads to an inhomogeneous force distribution and a resulting net force on each coil. This is due to the different local coil curvatures and the slightly helical arrangement of the coils. For different coil types there are different distributions of the magnetic force density. The average value of the magnetic force density over the coil cross-section yields radial and lateral force density components which vary along the circumference of the coils. The variation of the lateral force density component largely depends on the lateral excursion of the coil under consideration and is not very strongly influenced by the rest of the coils in the system.

In order to describe the forces, a local orthogonal coordinate system defined by the vectors **R**, **S**, and **T** is used, where **R** corresponds to the normal vector **n** of section 3, **S** is the binormal, and **T** the tangential vector. Hence, according to $\mathbf{f} = \mathbf{j} \times \mathbf{B}$, there are two components of the magnetic force density perpendicular to the direction of the current; f_R is the component in the direction of **R** (radial) and f_S the component in the direction of **S** (lateral). The component in the direction of **T** is zero ($f_T = 0$). In Figs. 5.1 to 5.5 the different distributions of the average force densities for the coils 1 to 5 of the system HSR 5-8 are shown versus the coil circumference (number of the General Current Elements – GCE –), beginning at the outboard side of the coils. The force distributions for the coils 6 to 10 are antisymmetric to those of the coils 1 to 5, according to the 'Stellarator symmetry' of the coil system. In Fig. 5.6 the force densities for coil 5 is calculated in more detail: The cross-section of the coil is divided into 3×3 microelements and the EFFI code deliveres spatial values of the force density. The magnitude of the lateral force density is comparable to the radial force density in certain regions, in particular, in coils with strong lateral excursions and strong local curvature. The average force densities of the four cases considered in Table II amount between $|\mathbf{f}| \approx 81$ MN/m^3 for the case with $R_0 = 18$ m and $|\mathbf{f}| \approx 51$ MN/m^3 for the case with $R_0 = 24$ m.

The coils generally exhibit overturning moments about the horizontal and vertical axes, and a torque about the coil axis (magnetic axis), with the overturning moments prevailing in magnitude. In the Figs. 5.7 and 5.8 the torques about the R-axis und the φ-axis for the coils 1 and 5 are presented as examples. The volume integral of the magnetic force

---

[27] Sackett, S.J., EFFI – A Code for Calculating the Electromagnetic Field, Force and Inductance in Coil Systems for Arbitrary Geometry, Lawrence Livermore National Laboratory Report UCRL-52402 (1978).

densities results in a net force for each coil in the coil assembly. The moderate helicity of the magnetic axis of Helias coil systems causes a related helicity in the net coil force vector, corresponding to different coil forces in the radial and vertical directions. These resulting net forces are shown in Fig. 5.9. Some coils even feel a force directed radially outward while others experience also a force component in the vertical direction which leads to a torque within each field period. The maximum net coil force is about 130 MN for an average major radius of $R_0 = 20$ m. The net force on the whole period (about 320 MN) is directed towards the torus center, and the net vertical forces vanishes, due to the 'Stellarator symmetry' of the coil system. It is of interest to compare these data with the centripetal forces of a system with equivalent circular planar coils on a circular magnetic axis with a major radius of 20 m. In such a case the net radial force per coil would be 63 MN [28]. This is due to the fact that in HSR 5-8 the maximum local curvature at the 'corners' of the configuration is about twice that of the circular system.

5.3. Mechanical stress and strain analysis

The detailed local magnetic force density distributions are the input data for the stress analysis. Stresses depend on the support system of the coils, which must be optimized with regard for material limits, engineering safety factors and a minimization of the structure material. Detailed stress and strain computations have been made for HSR 5-8 with a major radius of $R_0 = 20$ m. The coils of HSR 5-8 must be surrounded by a stainless steel housing since the virial stress is rather large. Studies with various dimensions of this housing and the location of inter coil support elements have been made using the computer code SUPPORT, as pre-processor to the finite-element calculations. This programme system subdivides the coils and generates the elements of the coil housing and mutual support. Local reinforcement of the structure in the radial and lateral directions, as well as trapezoidal elements are possible. Also the boundary elements can be defined with this code. The force densities mentioned above are transformed into nodal forces of the finite elements by means of shape functions [29].

For a typical case coil housing thicknesses of 35 cm at the outer coil face, and of 20 cm at the three other sides of the coil are assumed, with local reductions at the inner coil face to 15 cm in order to spend more space for blanket and shield at this locations. Stress maxima tend to arise where the coils are curved, and therefore extra reinforcement is provided in these areas. Support elements are located between adjacent coils; these are mainly confined to the region towards the torus center, thus leaving the outer region accessible for maintenance. Figure 5.10 shows the arrangement of these support elements for HSR 5-8 in a perspectivic view, Fig. 5.11 the same in the $\varphi - \vartheta$-plane of angular coordinates.

---

[28] Harmeyer, E., Analytische Lösungen für die Feld-, Stromdichte-, Kraftdichte- und die mechanische Spannungsverteilung in toroidalen Spulensystemen, Report IPP 2/294 Mai 1988.

[29] Gorenflo, H., Jandl, O., Calculation of the Nodal Forces in the 20-node Isoparametric Three-Dimensional Solid Element by the SHAPE Computer Program, Report IPP 4/167, March 1978.

It is difficult to predict for a future HSR the material data for the winding pack which would consist of superconducting strands, copper, aluminium alloy, stainless steel and insulating material. Tests must be made to obtain a reliable data base. For this report the orthotropic elastic data of two different conductors are used as first approximations for the compound:

- ABB-conductor, as discussed in section 5.1.
- ITER conductor, as proposed in [30], utilizing more steel for an increased stiffness of the coil winding pack.

The data are listed in Table IV and Table V.

Table IV: Elastic data of the ABB conductor

Young's modulus	$E_R = 21.3$ GPa, $E_S = 21.3$ GPa, $E_T = 37.0$ GPa
Shear modulus	$G_{RS} = 2.0$ GPa, $G_{ST} = 8.6$ GPa, $G_{RT} = 8.6$ GPa
Poisson's ratio	$\nu_{RS} = 0.1$, $\nu_{TR} = 0.317$, $\nu_{TS} = 0.317$

Table V: Elastic data of an ITER conductor

Young's modulus	$E_R = 42.0$ GPa, $E_S = 37.3$ GPa, $E_T = 70.7$ GPa
Shear modulus	$G_{RS} = 1.6$ GPa, $G_{ST} = 14.5$ GPa, $G_{RT} = 16.3$ GPa
Poisson's ratio	$\nu_{RS} = 0.14$, $\nu_{RT} = 0.29$, $\nu_{TS} = 0.15$

The elastic data of the coil housing and the support elements are those of stainless steel: E = 210.0 GPa, $\nu = 0.3$.

The SAP V(2) finite-element code is used to compute the stresses and strains of the system. One period of the coil system with 10 coils is modelled by 6344 elements and 9600 nodes. Each individual coil is represented by 480 elements, 96 per winding pack and 480 per housing; the remainig elements model the support structure. Since gap elements cannot be treated by SAP V(2) a rigid mechanical contact is assumed between the winding pack and the coil housing. Thus the calculations are linear. Fixed boundary conditions are defined at both ends of the period by the code SUPPORT, thus balancing the net force on the coils and the torque in one period (see Fig. 5.10). Because of the non-planar geometry of the coils and the inhomogeneous forces, all components of the stress tensor are equally important. The stresses are calculated in the center of each element; local stress maxima are approximately handled as well, using a local enhancement factor.

[30] Borokov, A.I., et al., Three Dimensional Finite Element Stress Analysis of Different Designs of Superconducting Toroidal Field Coils for the International Thermonuclear Experimental Reactor, IEEE Transactions on Magnetics, Vol.28, No.1, (1992), 247.

Figure 5.12 shows as a result of the finite-element calculations the displacements for the whole field period. In Figs. 5.13 to 5.18 these displacements in radial, lateral and tangential direction as well as the magnitude of the averaged displacements of the coils 1 to 5 are presented. The results show that the coils tend to become more circular and planar under the magnetic load. This causes bending stresses and related shear stresses in the coils. The maximum displacement value occurs in coil 1 at the outer side, see Fig. 5.13 and Fig. 5.12, and amounts to about 30 mm. In Fig. 5.17 in comparison to Fig. 5.18 the displacements of the coils 5 and 46 are shown; the antisymmetry of these two coils due to the 'Stellarator symmetry' of the coil system is clearly visible.

In Figs. 5.19 to 5.24 the results of the stress calculations are given. The normal stress components σ_R, σ_S, σ_T and the shear stress components σ_{RS}, σ_{ST}, σ_{TR} of the winding pack of the 10 coils in one period (coil 46 to coil 5) are presented as a function of the coil circumference. In these computations the elastic data of the ABB conductor from Table IV are used. In the figures, again, the 'Stellarator symmetry' of the coil system is visible, i.e. the curves for the coils 1 to 5 are antisymmetric to those for the coils 46 to 50. Of course, this result shows, on the one hand, that there is a redundancy in the computations; on the other hand, this method simplifies the choice of boundary conditions in the calculations: The boundary conditions has been justified in calculations for the Wendelstein 7-X experiment. In that computations a new set of boundary conditions was defined by shifting the modul by half a period [31], with reasonable agreement in the results.

The maximum stresses for the coil winding pack of HSR are found to be $\sigma_T \approx 54$ MPa and $\sigma_{ST} \approx 13$ MPa, see Fig. 5.21 and Fig. 5.23. These values are valid for the compound, according to the data of Table IV. In order to obtain the stress values in the aluminium alloy which mainly carries the magnetic load the percentage of it ($\approx 50\%$) has to be considered. Furthermore, the increase of tensile stress at the surface has to be taken into account. For these reasons a local enhancement factor of 2.4 is assumed. Using this enhancement factor maximum stresses for the aluminium alloy of $\sigma_T \approx 130$ MPa are estimated which is far below the expected yield stress of $\sigma_{0.2} \approx 350$ MPa for this material [32]. A maximum shear stress for the insulation of $\sigma_{ST} \approx 30$ MPa is attained which is considered to be within the safety margin. These stress maxima are rather localized and it is expected that a further reduction is possible by optimizing the support system.

The stress distribution for the stainless steel coil housing of coils 1 and 5 is shown in the Figs. 5.25 and 5.26, again versus the coil circumference. In these figures the stress component σ_T clearly exhibit the axes and the locations where the coils are subjected to bending. The maximum equivalent stress (von Mises stress) for the coil housing is found for coil 5 and amounts to about $\sigma_{vM} = 530$ MPa, also far below the value of yield stress of $\sigma_{0.2} \approx 820$ MPa for stainless steel at 4 K.

---

31) Harmeyer, E.,: Comparisation of W 7-X Coil Configurations in View of Forces and Stresses, Proceedings of the 5th Ringberg Workshop on W 7-X, June 1992, IPP 2/317, 117ff.

32) Harmeyer, E., Schoenewolf, I., et al., Die Supraleiter-Testspule für W 7-X in der Anordnung STAR von KfK, Report IPP 2/315, Jan. 1992.

The strain distributions for the coil winding pack are given in Figs. 5.27 to 5.32 as results of the stress calculations using the orthotropic elastic data of the ABB conductor from Table IV. The normal strain components ε_R, ε_S, ε_T and the shear strain components γ_{RS}, γ_{ST}, γ_{TR} of the winding pack of 5 coils of one period (coil 1 to coil 5) are presented as a function of the coil circumference. In Fig. 5.33 the distribution of the tangential strain component ε_T for the coil housing of coils 1 and 5 is illustrated. Peak values of more than 0.2% are seen at few positions, but it is expected that these values can be reduced by further optimizing the support system.

Using the elastic data of Table V for an ITER conductor which utilizes more steel for the coil winding pack and keeping the geometry of the system unchanged, we find increased stress values in the winding pack and decreased values for the coil housing, as expected. In Figs. 5.34 to 5.36 some results of these calculations are given. The normal stress component σ_T (see Fig. 5.34) and the shear stress component σ_{TR} (see Fig. 5.35) of the winding pack of the 10 coils of one field period are shown versus the coil circumference. Compared to the former results of the Figs. 5.21 and 5.24 these values are increased by a factor of about 2. The associated stress distribution for the coil housing of coil 1, as shown in Fig. 5.36, exhibit a decrease of stress values of about 20% compared to those of the former calculations for coil 1, as shown in Fig. 5.25. The latter result calls for applying reduced dimensions for the coil support system, when introducing more steel in the coil winding pack.

Between the coil winding pack and the coil housing a rigid mechanical contact is assumed in the computations. In a real system no tensile stress can be transfered between these components. This 'contact problem' has been treated for the Wendelstein 7-X coil system [33) 34)], using the ADINA code. Gap elements are introduced in the coils along the coil circumference. The results indicate an increase up to about 30% of the von Mises stress, using gap elements of 5 mm thickness minus 0.5 mm free space. Specific components of the stress tensor, particularly the normal stress components in radial and lateral direction, increase while other components decrease as these gap elements are taken into account. It is believed that this general result can be applied for HSR also.

At initial condition of the above calculations the coil system is considered to be cold, free of gaps and free of stresses. The stresses described above arise from magnetic forces only; those caused by cooling-down and manufacturing processes are not yet considered.

Acknowledgements

The contributions of W. Maurer, KfK-Karlsruhe, to this report are well acknowledged.

33) Simon-Weidner J., Jakšić, N., Harmeyer, E., On Mechanical Stresses in Large Helias Coil Systems and the Influence of Contact Effects, Proceedings of the 16th Symposium on Fusion Technology, London, UK, 1990, Vol.2, 1511-1514.

34) Jakšić, N., Simon-Weidner J., Harmeyer, E., On Mechanical Boundary Conditions in Large Helias Coil Systems and the Influence of Sliding on Stresses, Proceedings of the 17th Symposium on Fusion Technology, Roma, Italia, 1992, to be published.

6. Summary and conclusions

In Helias configurations the plasma confinement and stability has been optimized. The theoretical predictions show that reactor-relevant parameters can be achieved in these configurations for neoclassical losses in addition to extrapolated anomalous ones.

One of the most relevant and complex components of a Helias reactor is the superconducting modular coil system; therefore extensive studies have been made on forces and stresses of the system. The electromagnetic forces are inhomogeneous with components in all directions. This inhomogeneous force distribution causes a complex stress and strain distribution inside the coils and the structure; but the magnitude of these values can be kept within technical limits by utilizing an optimized support structure. This support system consists of mutual support between adjacent coils; the coils of a toroidal field period are connected to a module. All coils thus comprise a common vault.

Using the material data of the conductor developed for the Wendelstein 7-X experiment as input for the winding pack, the results of the finite-element computations show that maximum tensile stresses are about $\sigma_T \approx 130$ MPa for the load carrying aluminium alloy of the winding pack. This value is well below the expected value of yield stress of $\sigma_{0.2} \approx 350$ MPa for the considered material. The maximum shear stress component acting mainly on the insulation of the winding pack amounts to $\sigma_{ST} \approx 30$ MPa, which is considered to be within the safety margin. The maximum stresses in the support structure of stainless steel is found at coil 5 and amounts to $\sigma_{vM} \approx 530$ MPa, equivalent to an expected safety factor of 1.55. The related values of the strain tensor in these computations are low and exceed a value of 0.2% only at few positions along certain coils. Using the material data of an ITER conductor with an increased fraction of stainless steel in the compound yields increased stress values in the compound and decreased ones in the coil housing, as expected.

The total mass of HSR of about 26 kt for the entire system with a major radius of 20 m and a fusion power output of 3 GW which is related to an electric power output of about 1.1 GW leads to mass utilisation of approximately 40 kWe/t which is an acceptable value in comparison to that of some tokamak reactors studies.

In summary, the superconducting modular coil system of a Helical Stellarator Reactor (HSR) seems to be feasible and offers the opportunity to operate the reactor with good economical prospects.

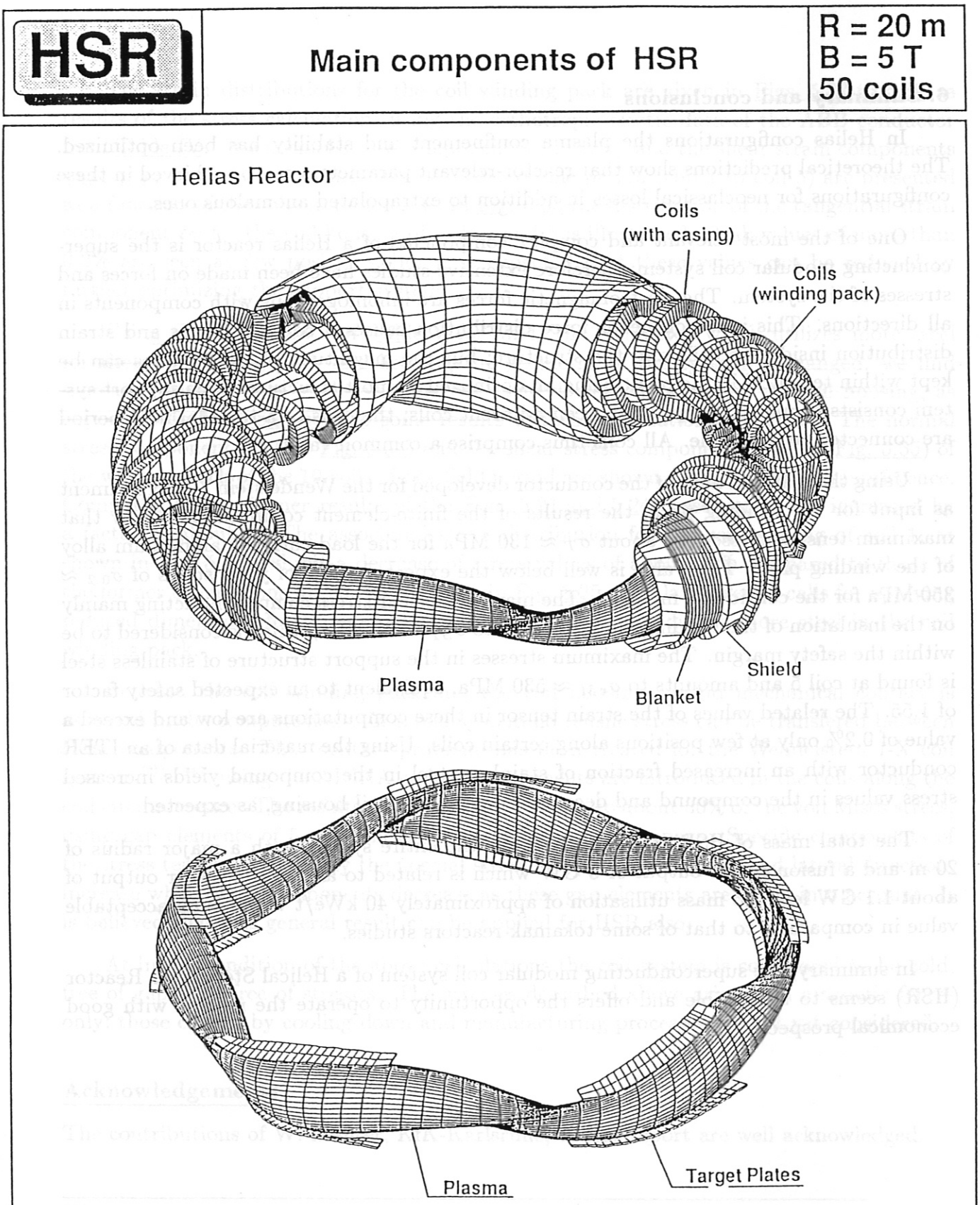

Fig. 2.1: Top: Main components of a Helias reactor.
Bottom: Magnetic surface and divertor target plates of a Helias reactor.

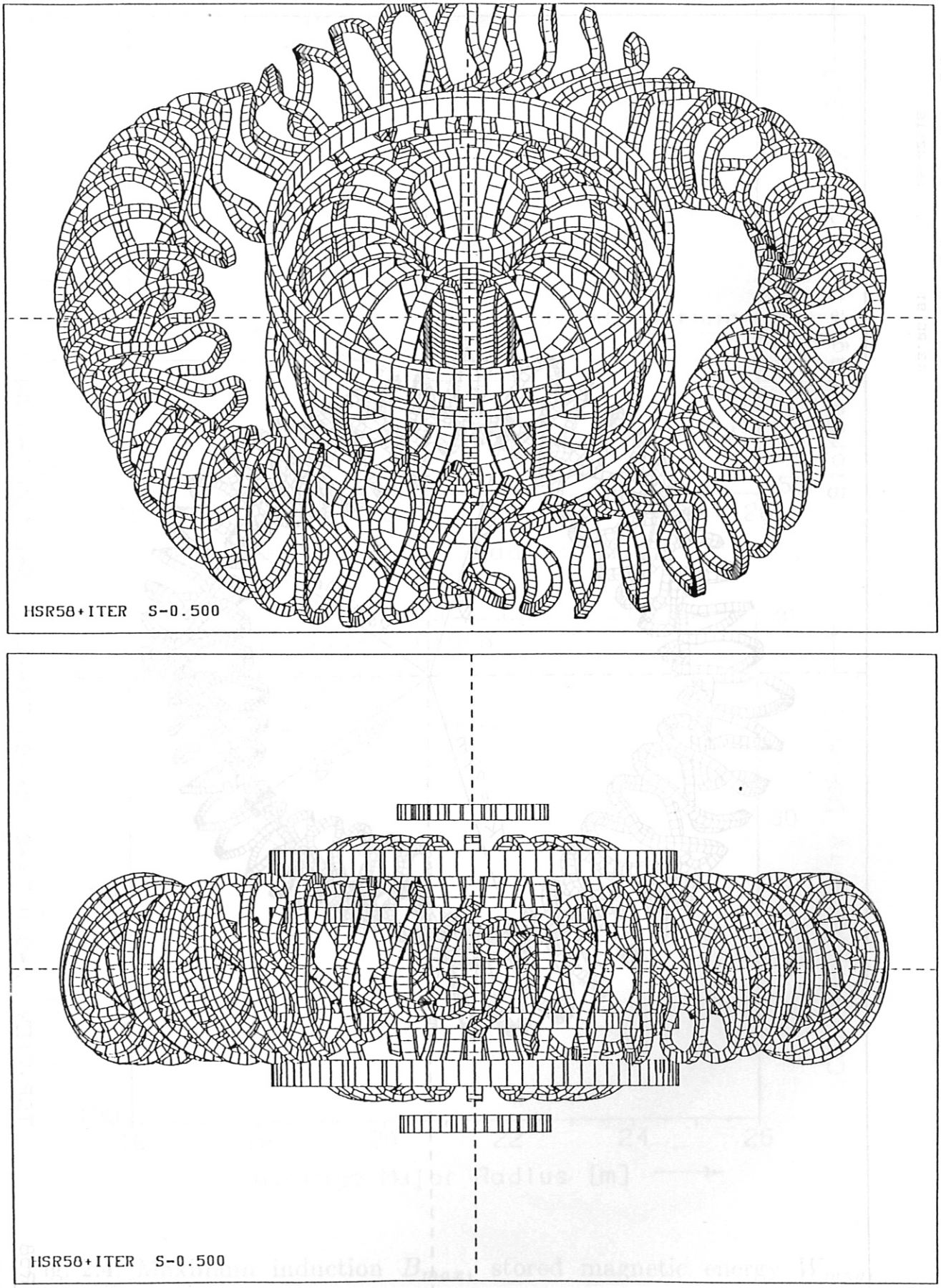

Fig. 2.2: Coil systems of ITER and HSR, HSR surrounding ITER.

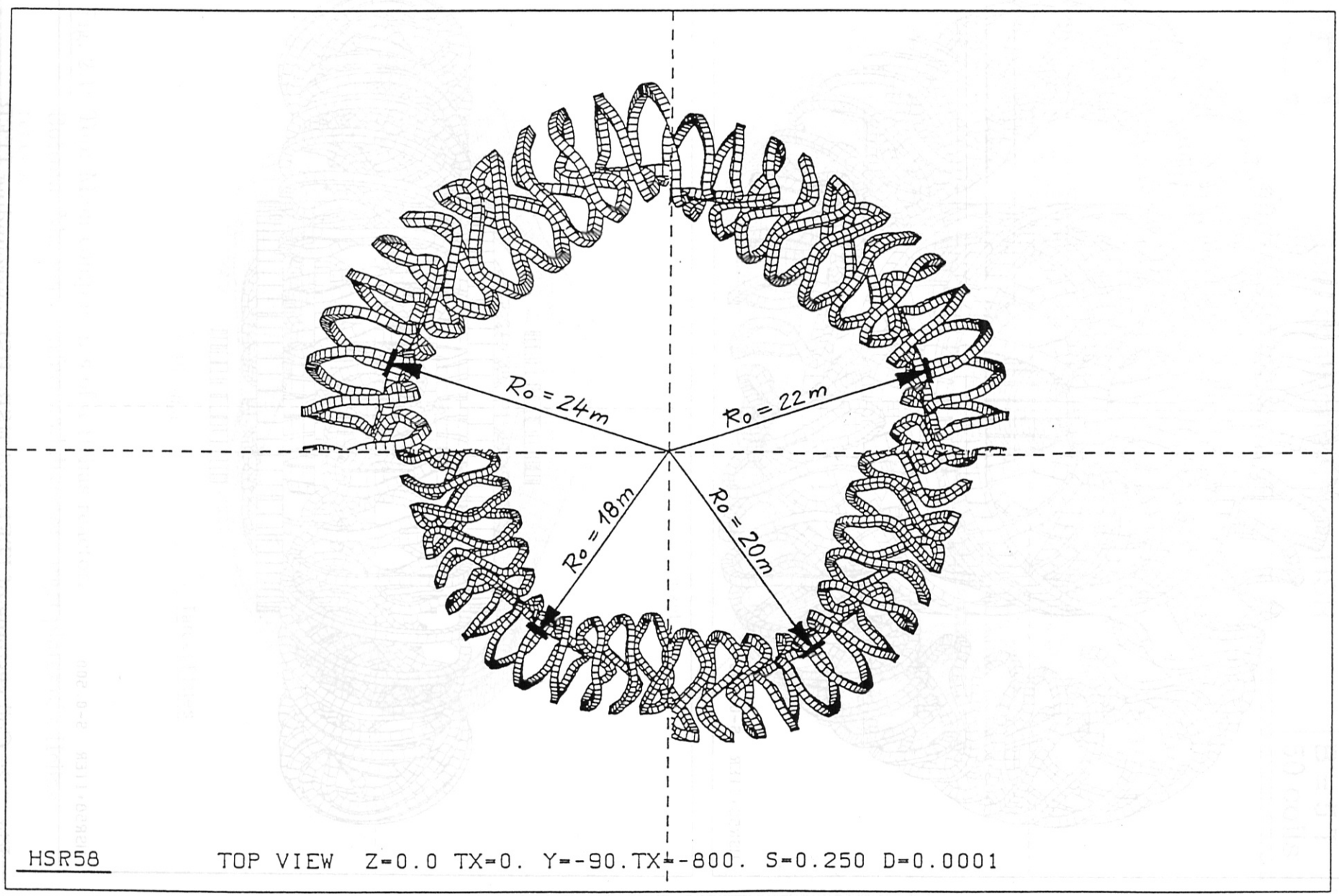

Fig. 2.3: Helias reactor HSR 5-8 with different major radii.

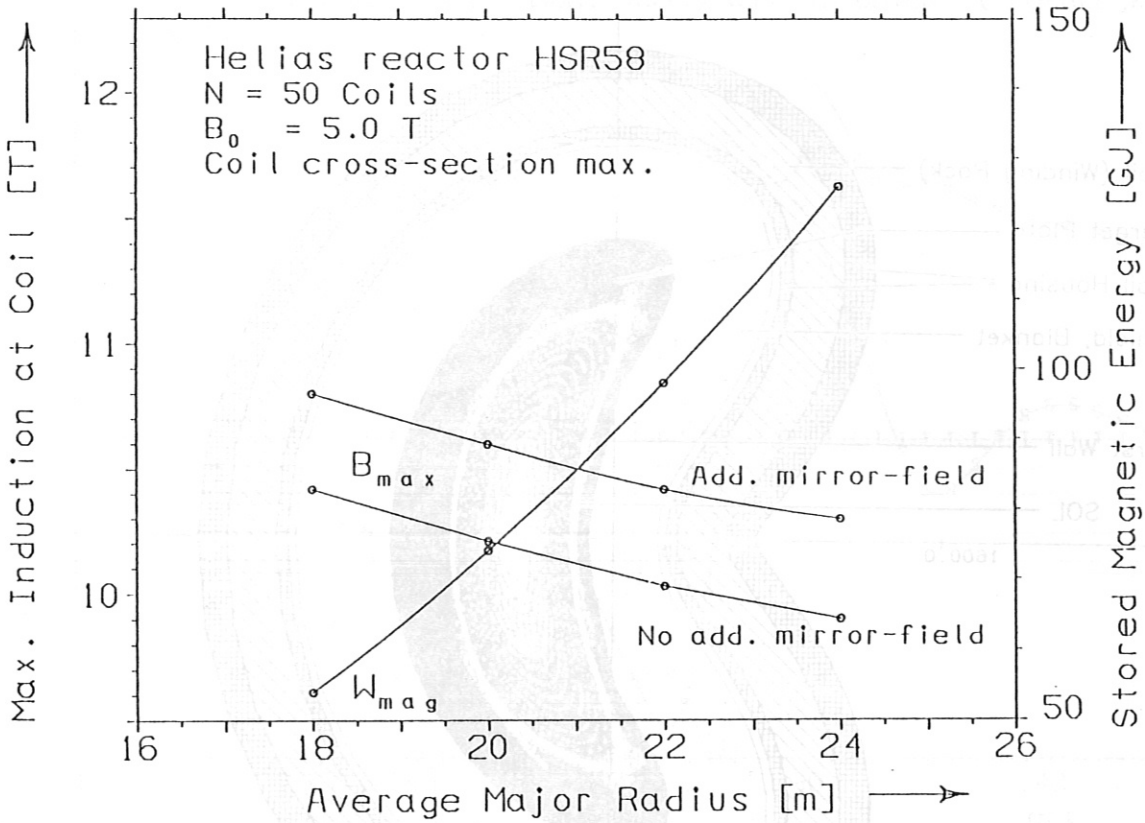

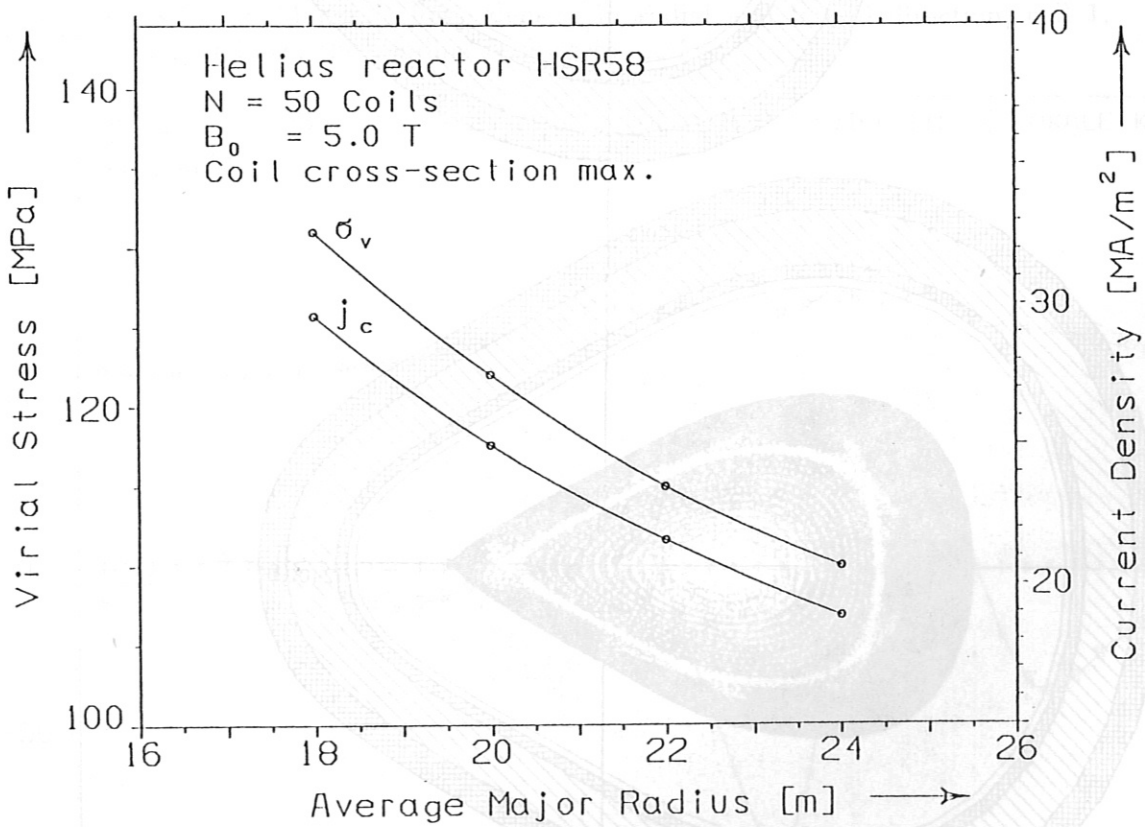

Fig. 2.4: Maximum induction B_{max}, stored magnetic energy W_{mag}, virial stress σ_V, and current density j_c, versus the major radius R_0 under the condition, that the coil cross-section is a maximum.

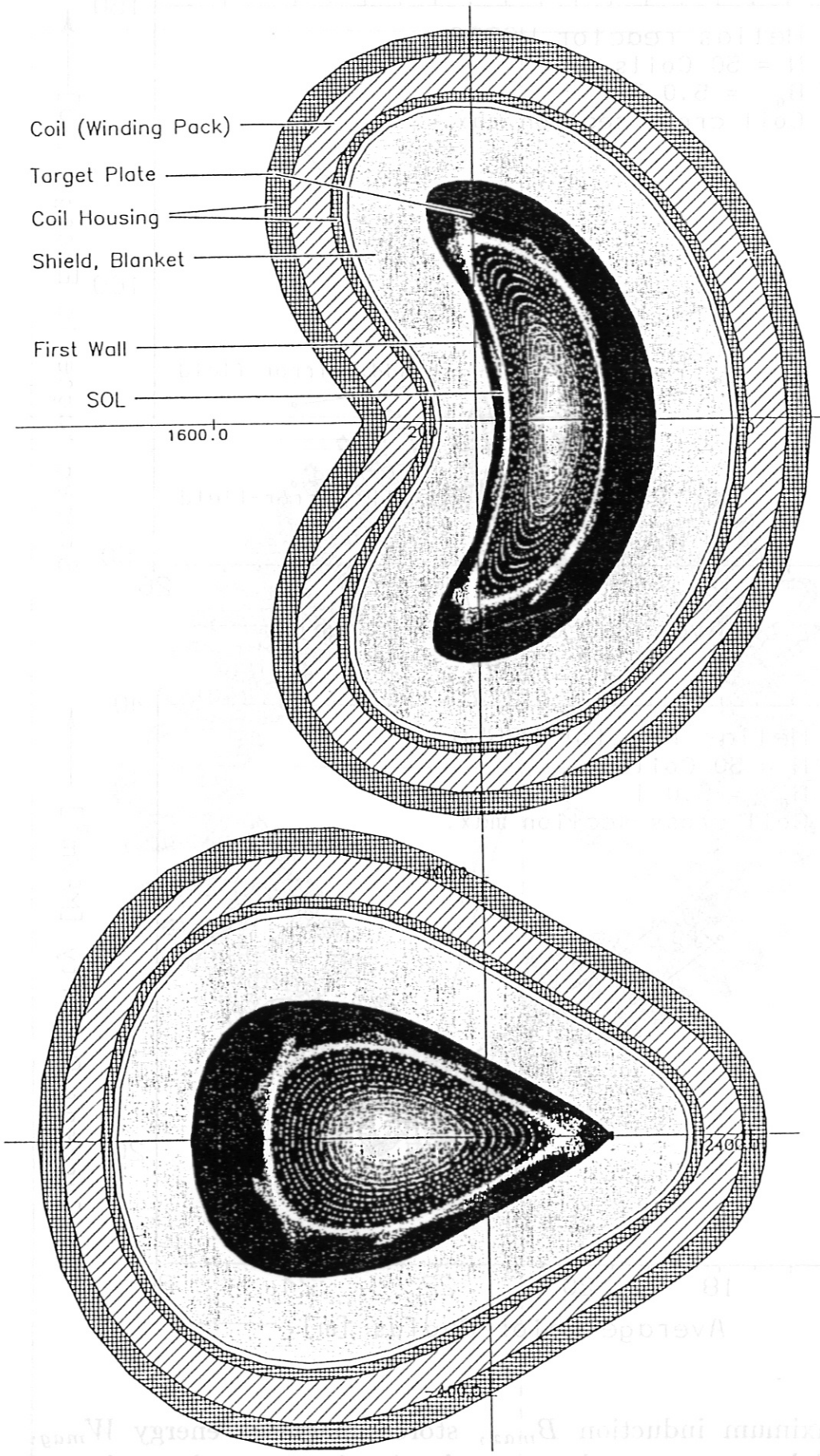

Fig. 4.1: Poincaré plot of vacuum magnetic surfaces for the configuration HSR 5-10 of 2 toroidal planes, $\varphi = 0^o$ and $\varphi = 36^o$, showing also the space for coil, blanket, shield, and divertor.

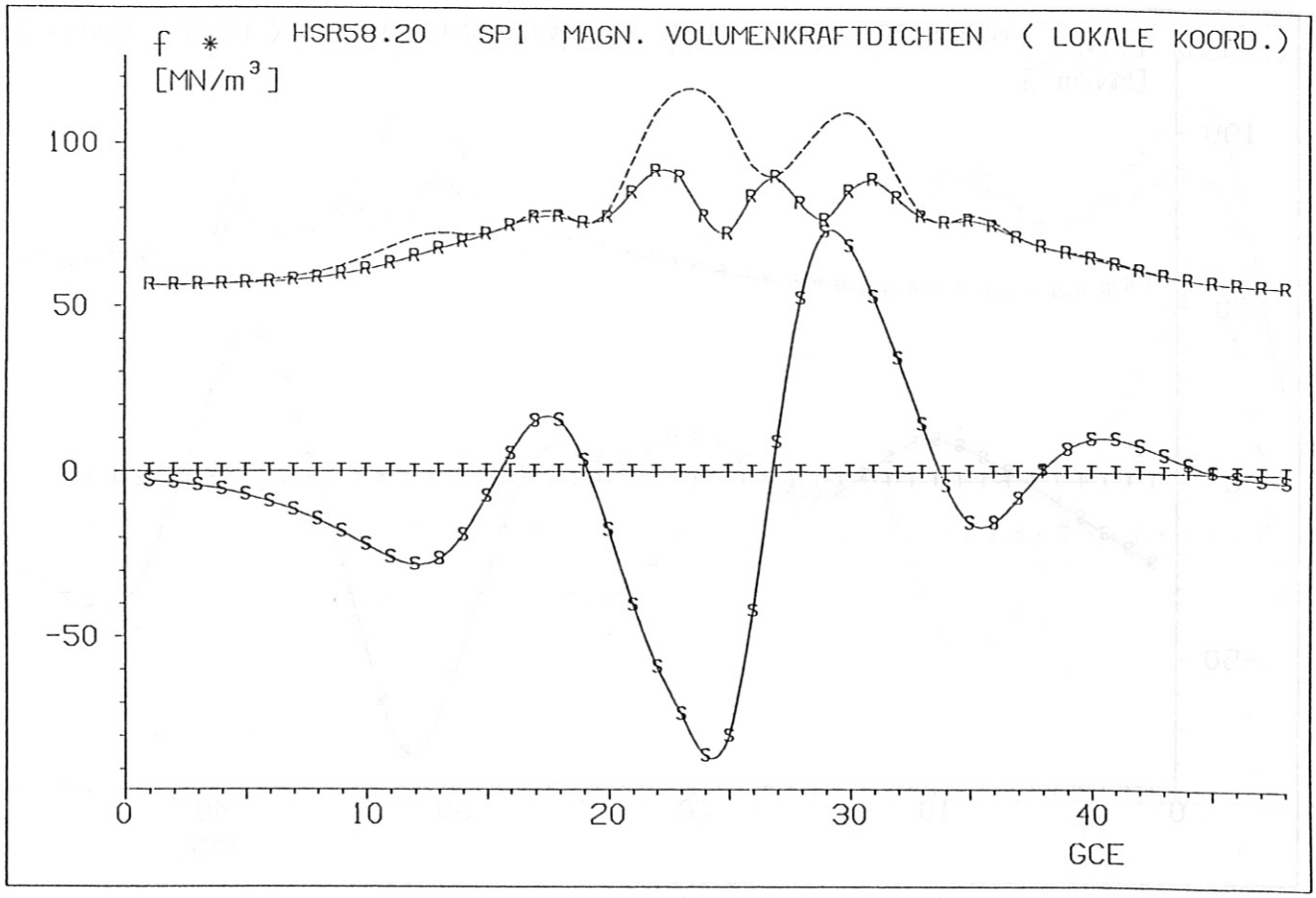

Fig. 5.1: HSR 5-8: Magnetic force density in radial and lateral direction, coil 1, averaged over the winding pack cross-section.

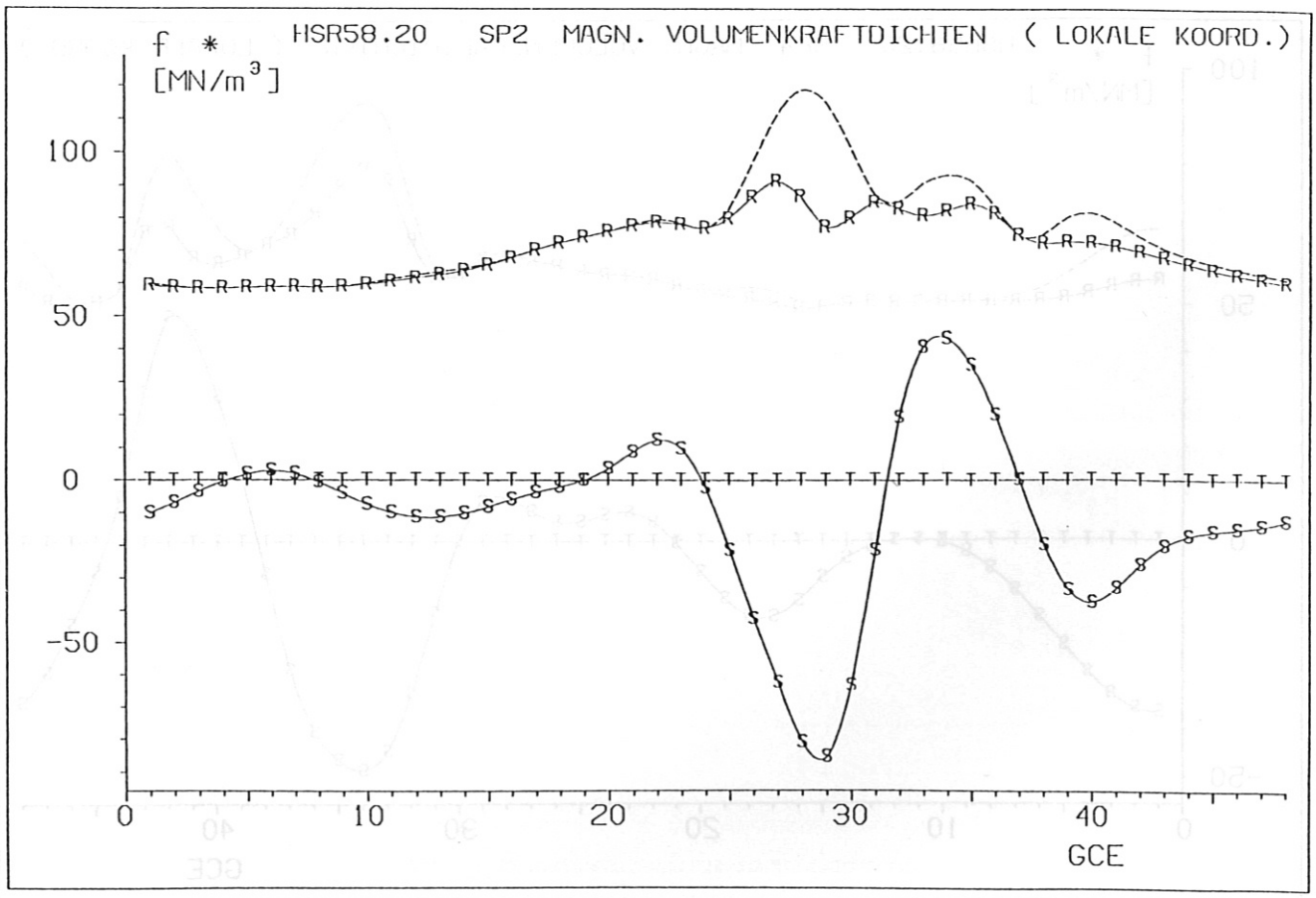

Fig. 5.2: as Fig. 5.1, coil 2.

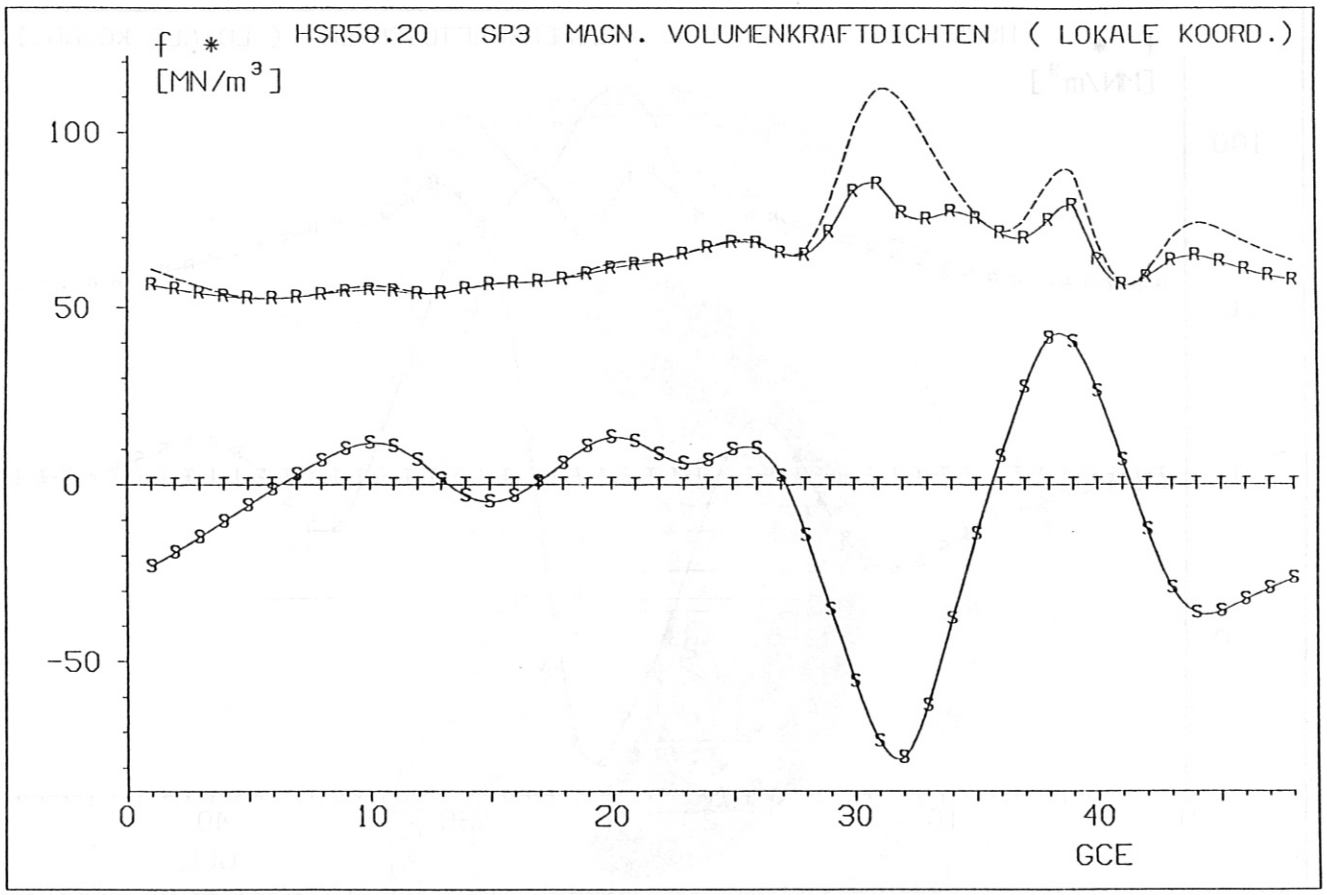

Fig. 5.3: HSR 5-8: Magnetic force density in radial and lateral direction, coil 3, averaged over the winding pack cross-section.

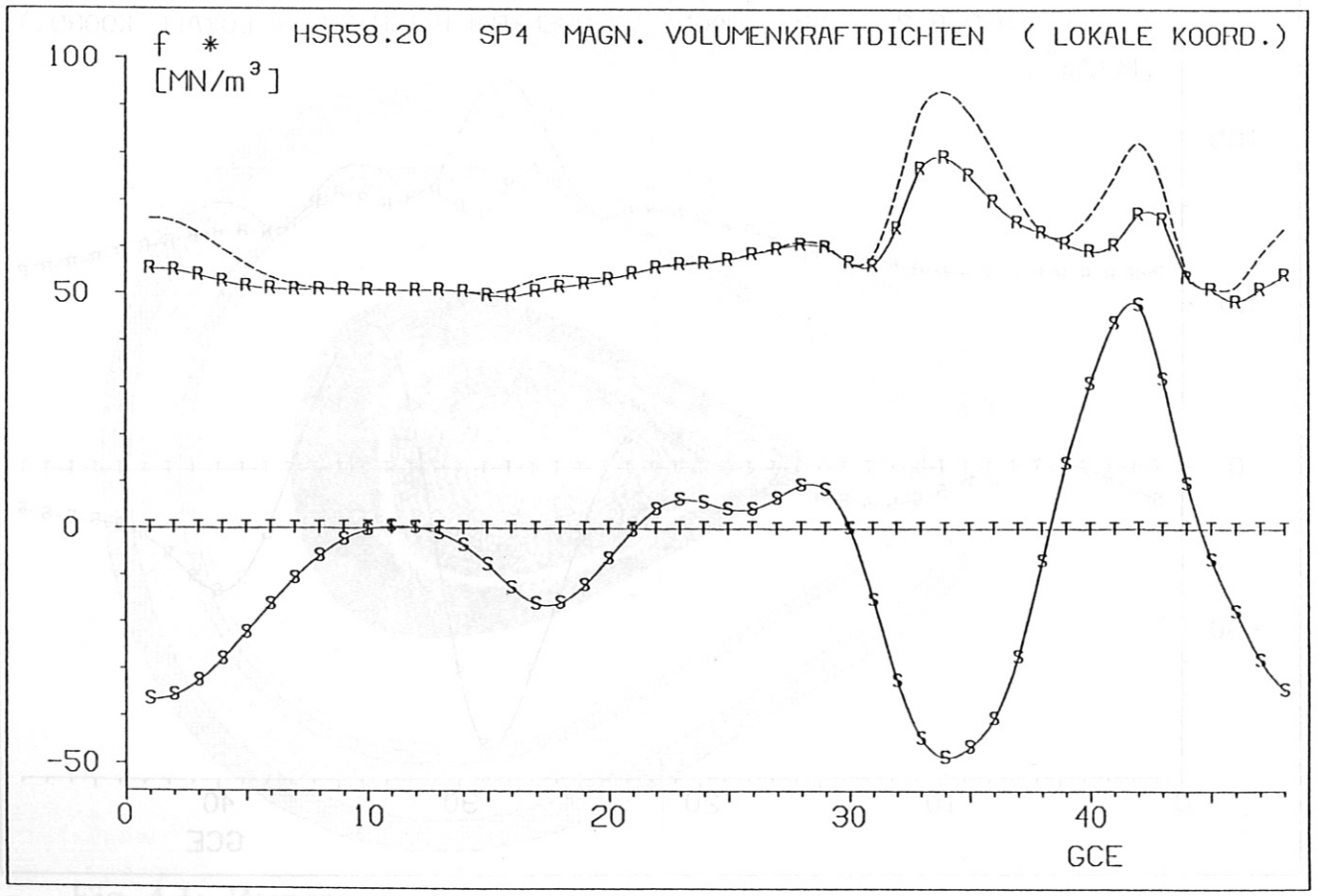

Fig. 5.4: as Fig. 5.3, coil 4.

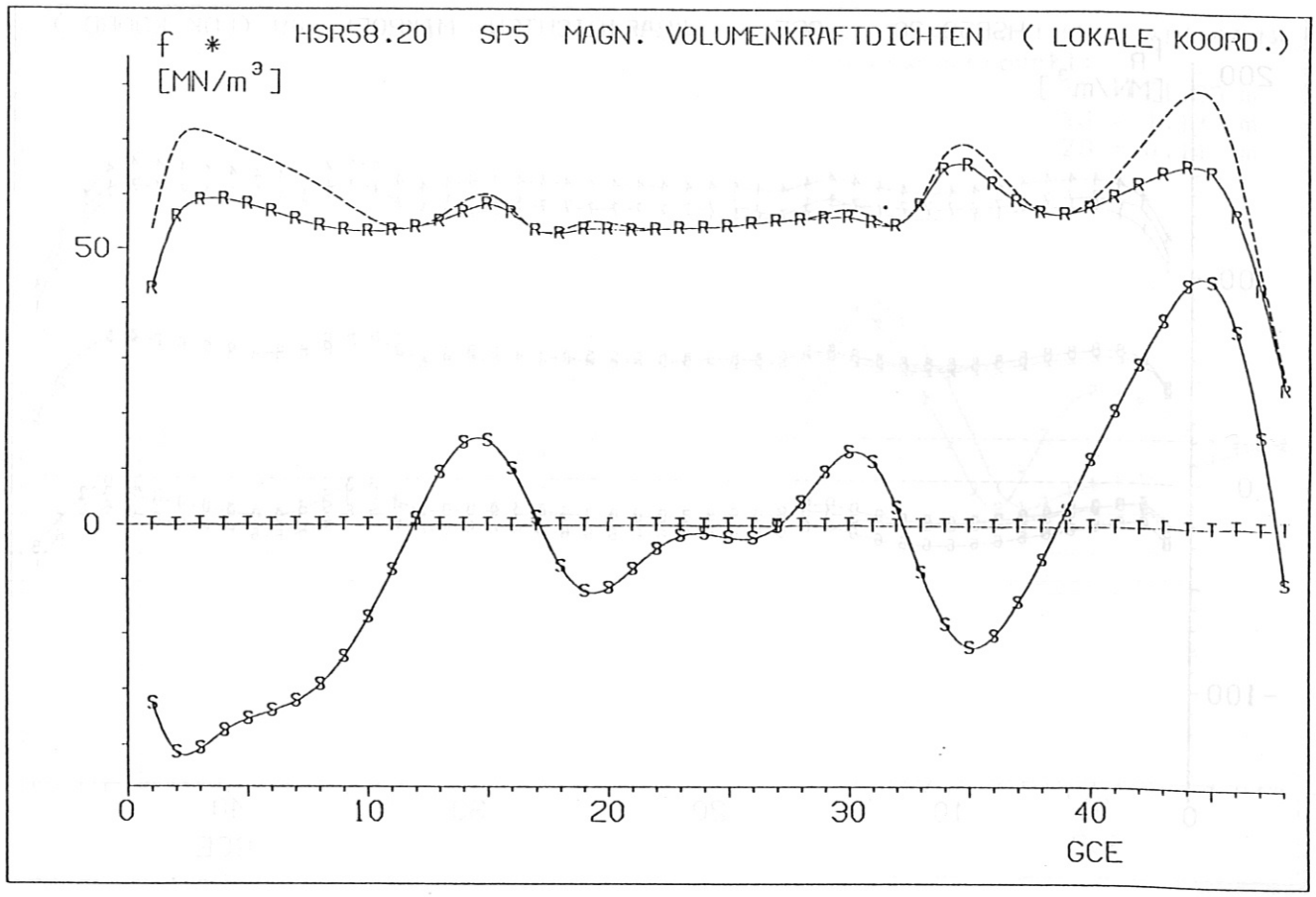

Fig. 5.5: HSR 5-8: Magnetic force density in radial and lateral direction, coil 5, averaged over the winding pack cross-section.

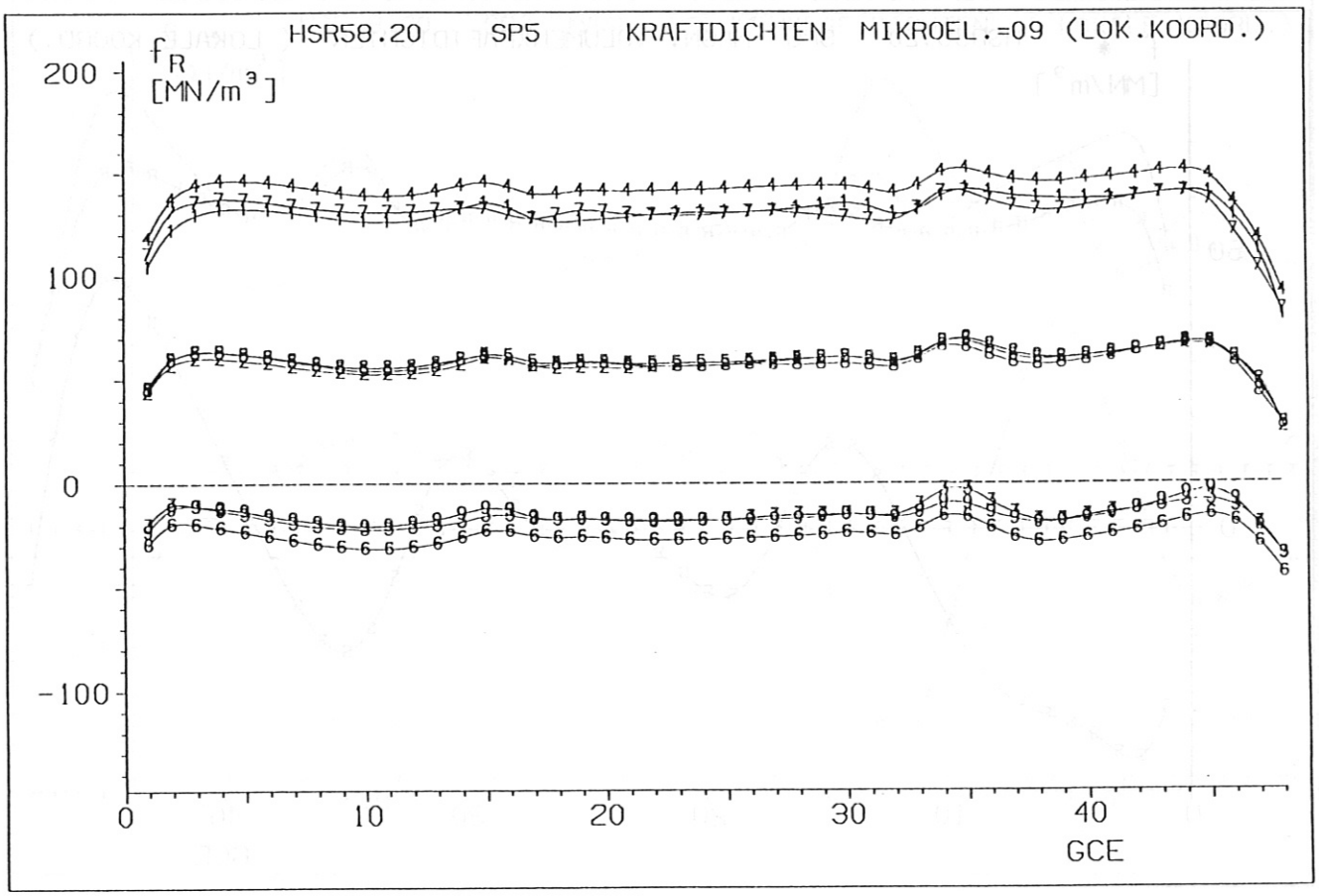

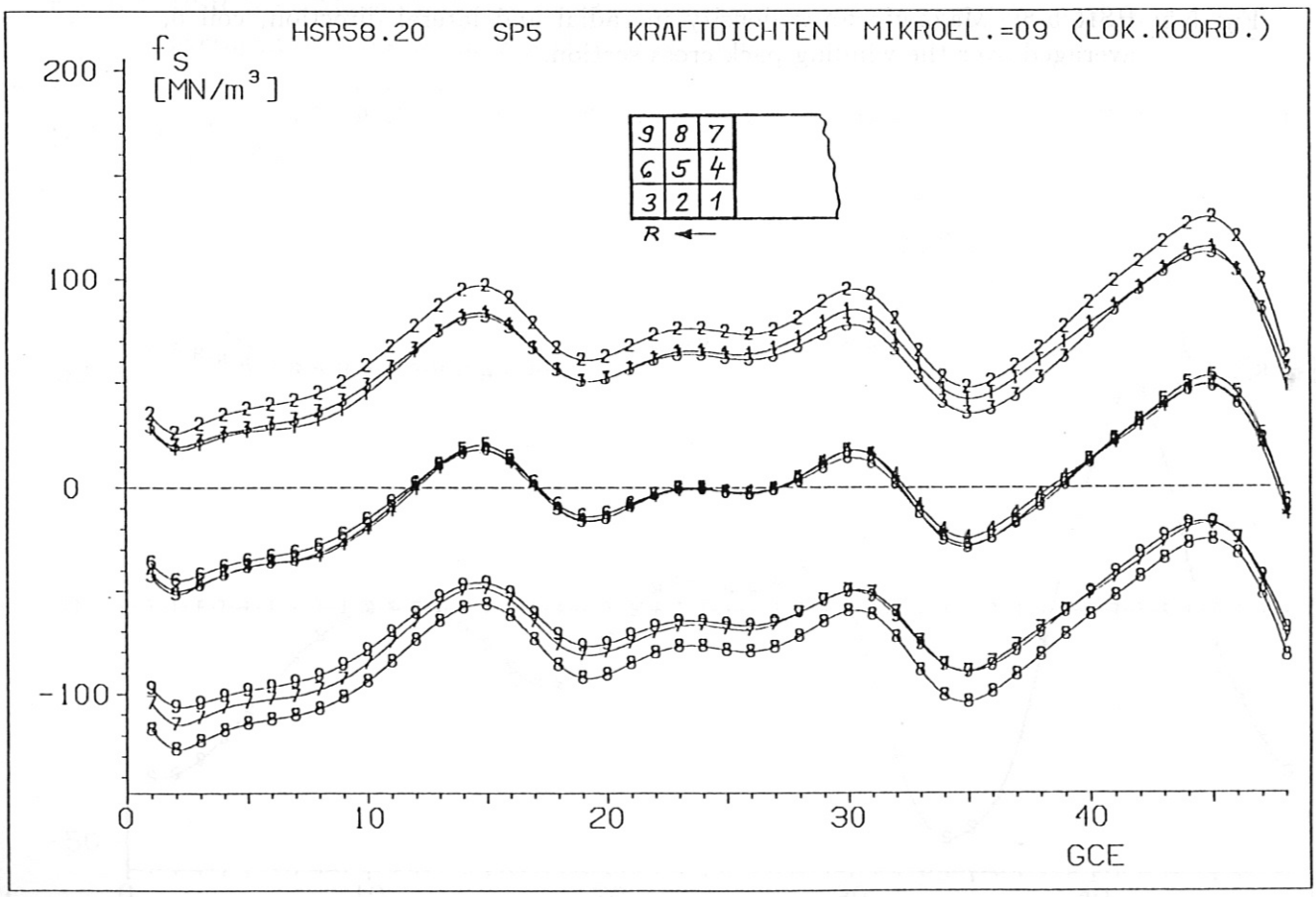

Fig. 5.6: HSR 5-8: Magnetic force density distribution in radial and lateral direction, coil 5. As shown in the insert the cross-section is devided into 3×3 microelements.

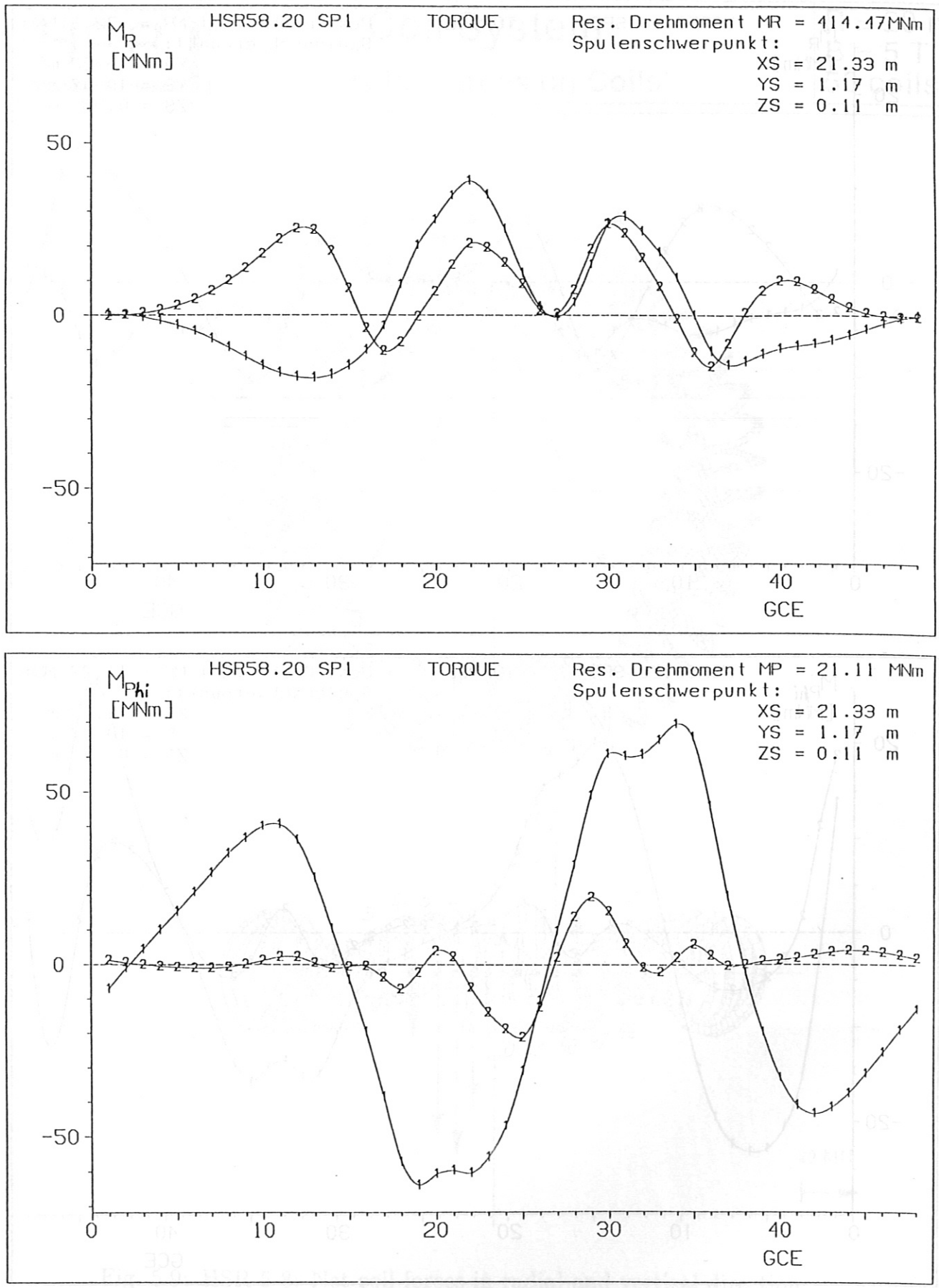

Fig. 5.7: HSR 5-8: Torque on coil 1 about the R-axis and φ-axis.

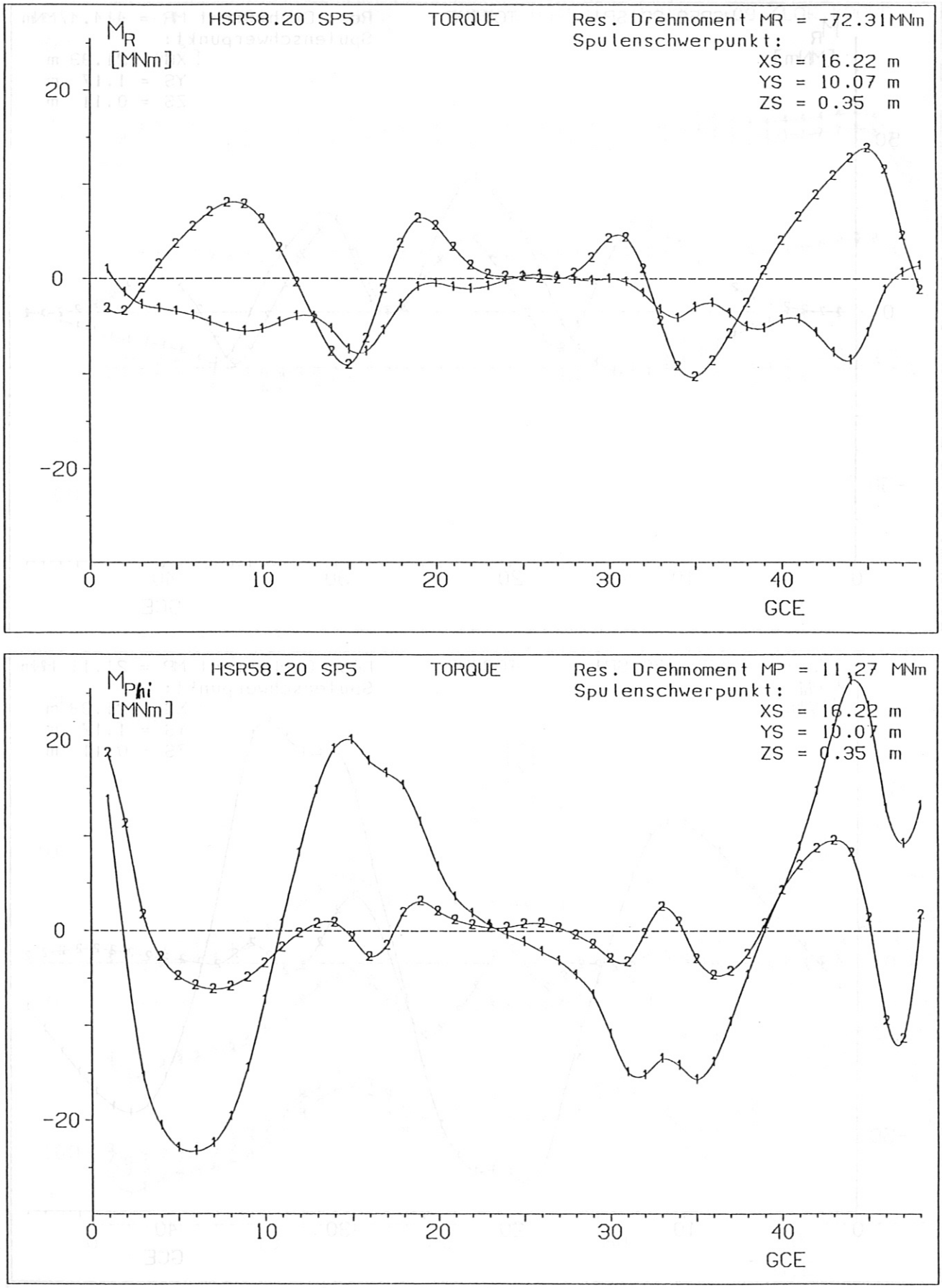

Fig. 5.8: HSR 5-8: Torque on coil 5 about the R-axis and φ-axis.

HSR

Coil System

Total Forces on Coils

R = 20 m
B = 5 T
50 coils

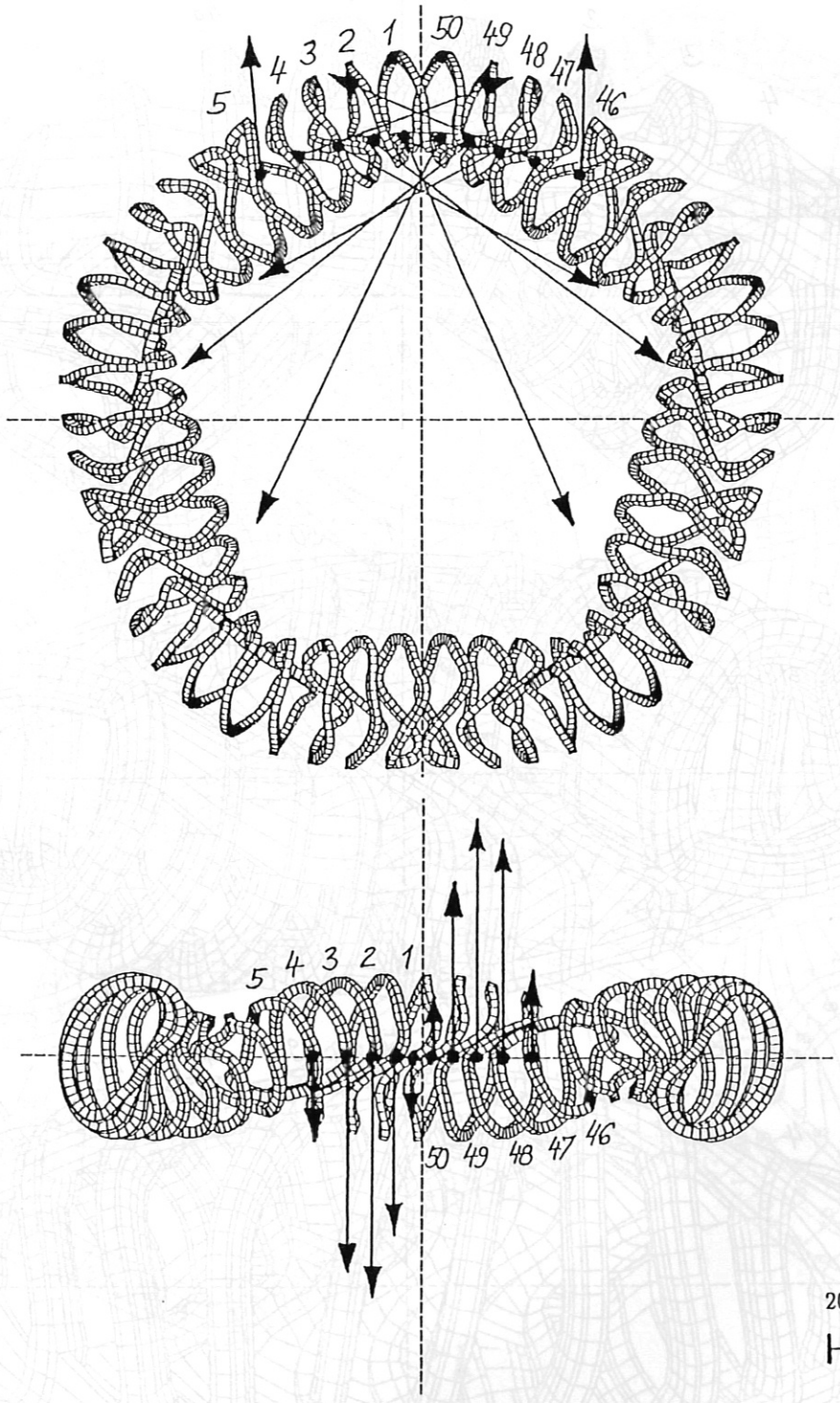

Fig. 5.9: HSR 5-8: Net coil forces in radial and vertical direction.

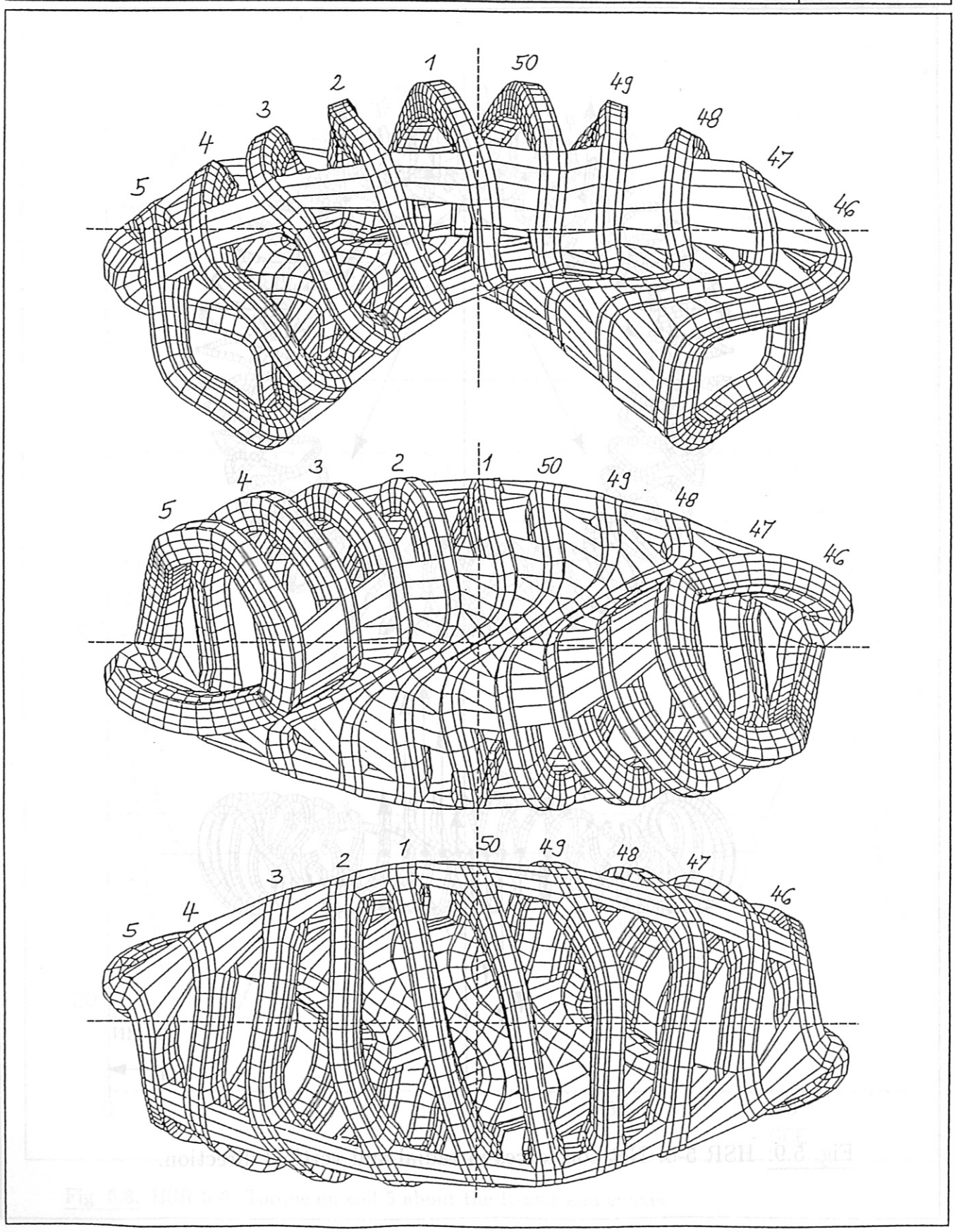

Fig. 5.10: HSR 5-8: Mutual coil support system.

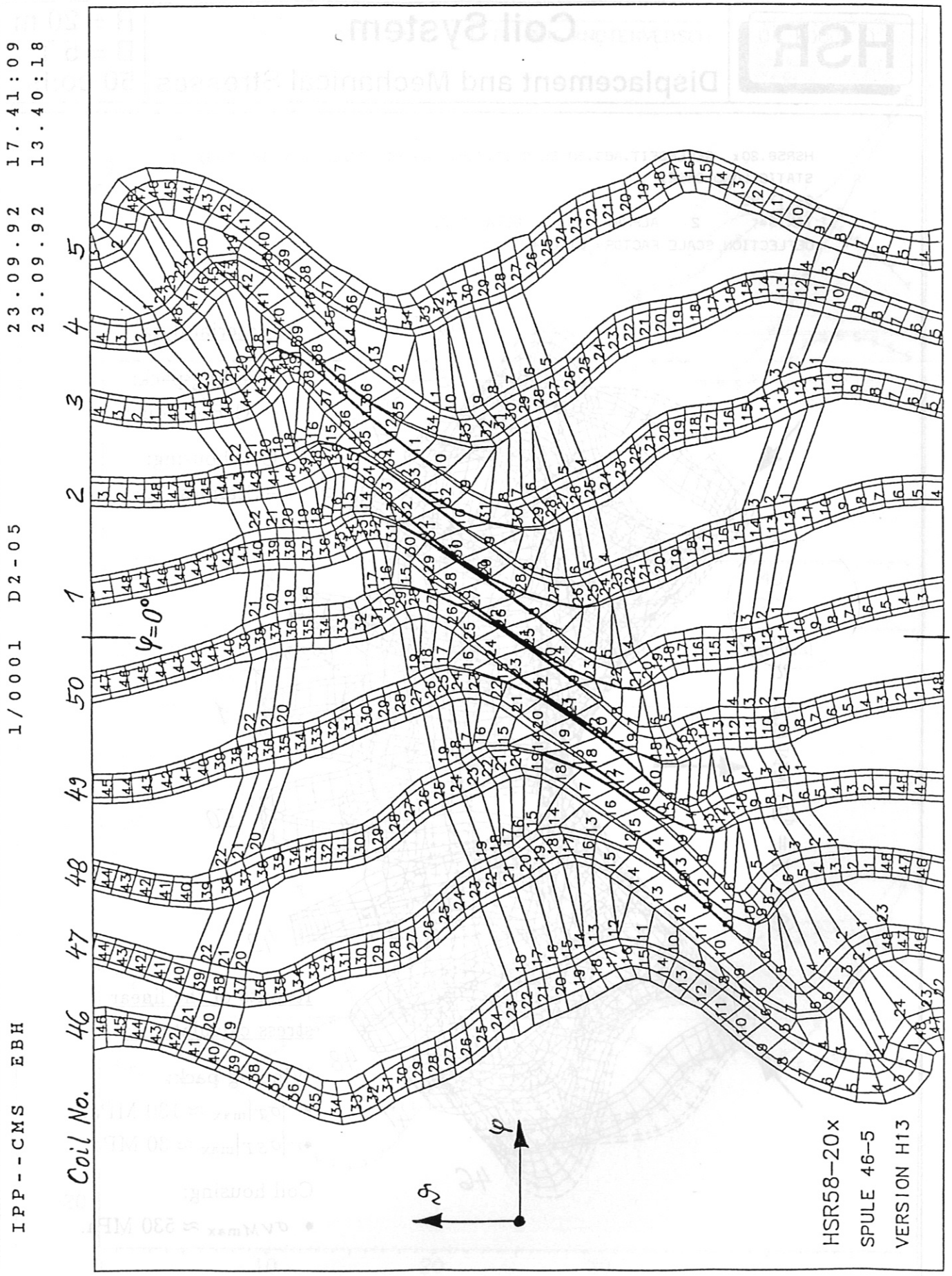

Fig. 5.11: HSR 5-8: Support system shown in the $\varphi - \vartheta$-plane of angular coordinates.

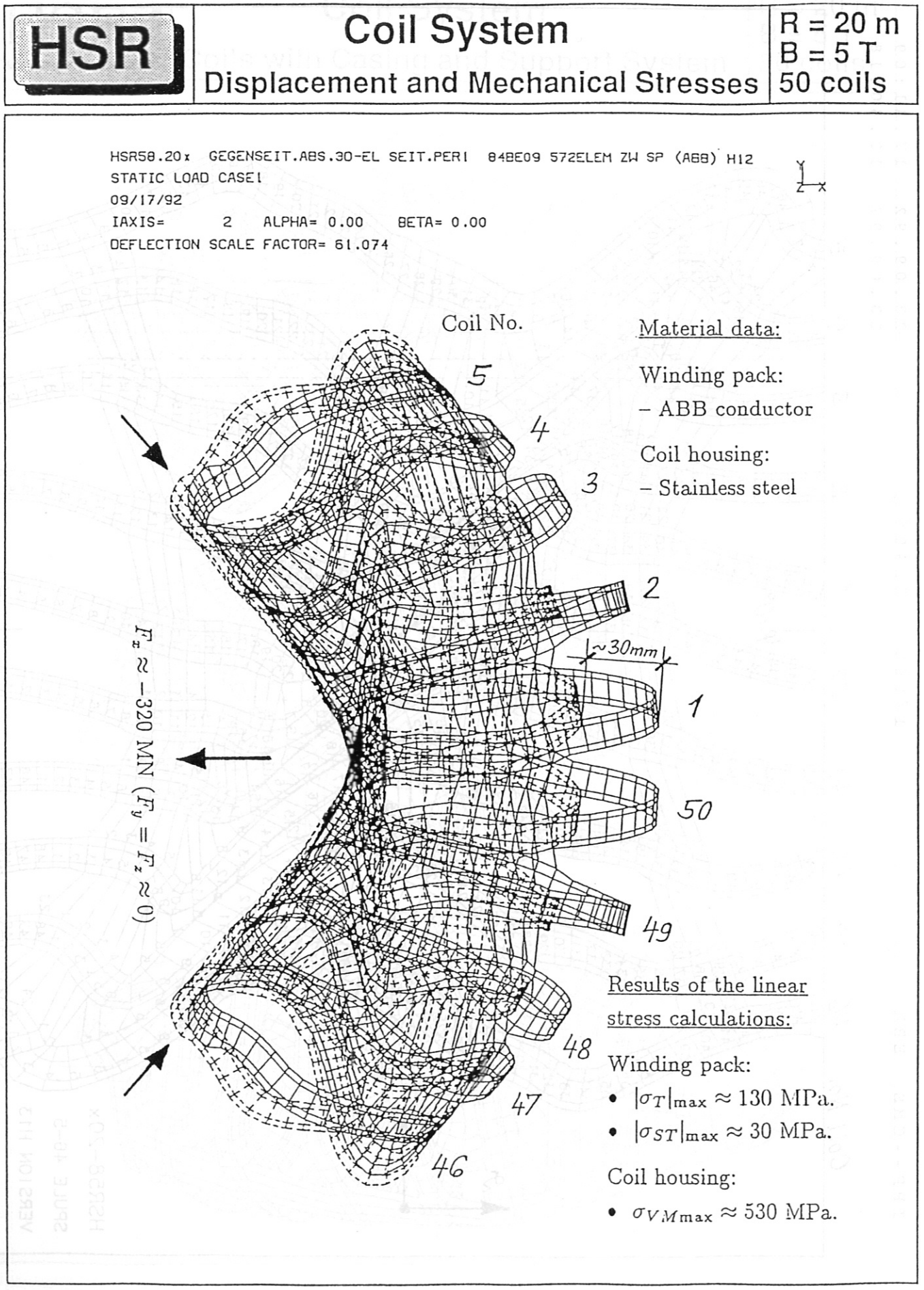

Fig. 5.12: HSR 5-8: Displacement plot.

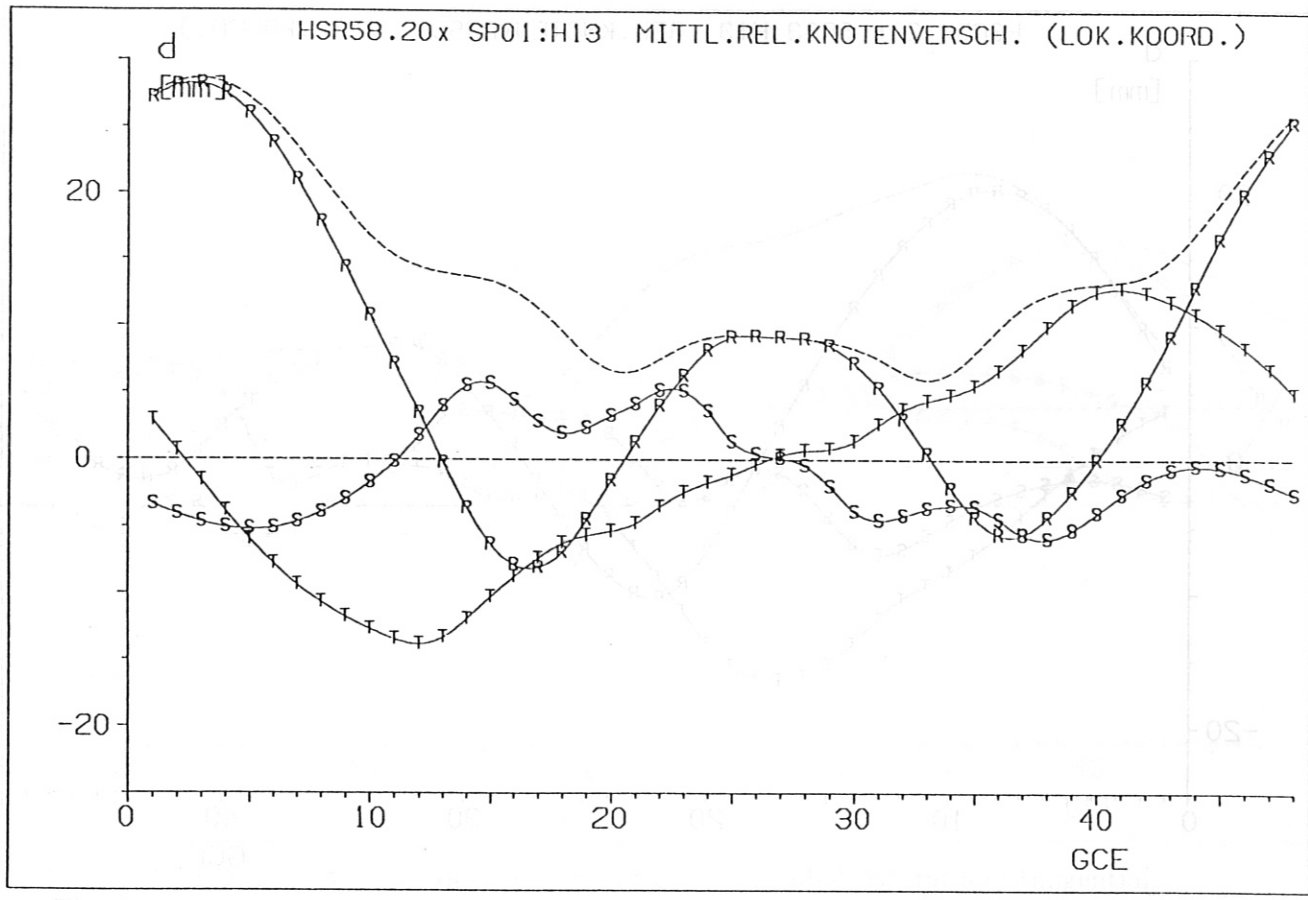

Fig. 5.13: HSR 5-8: Average displacement of coil 1 in radial, lateral and tangential direction.

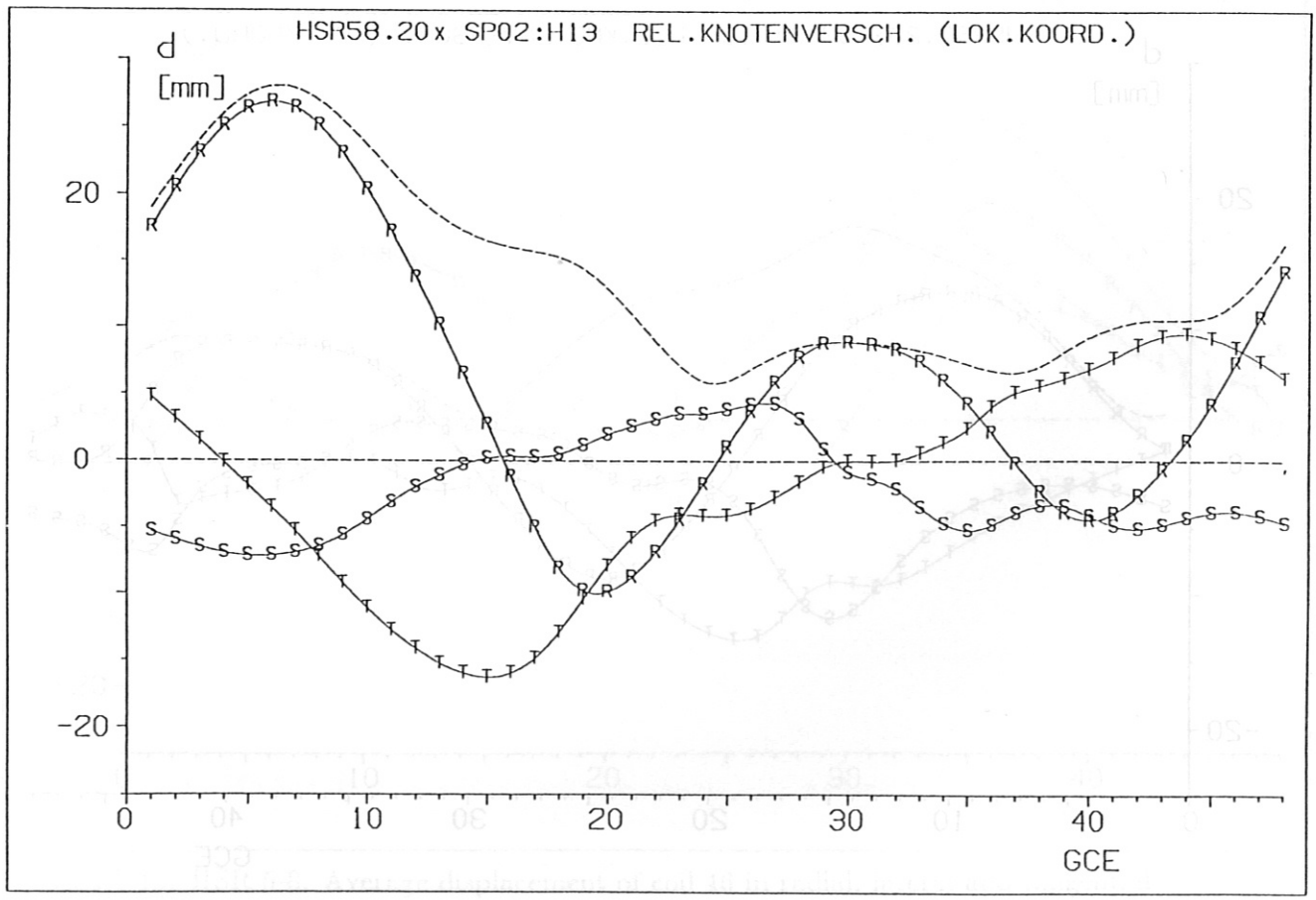

Fig. 5.14: as Fig. 5.13, for coil 2.

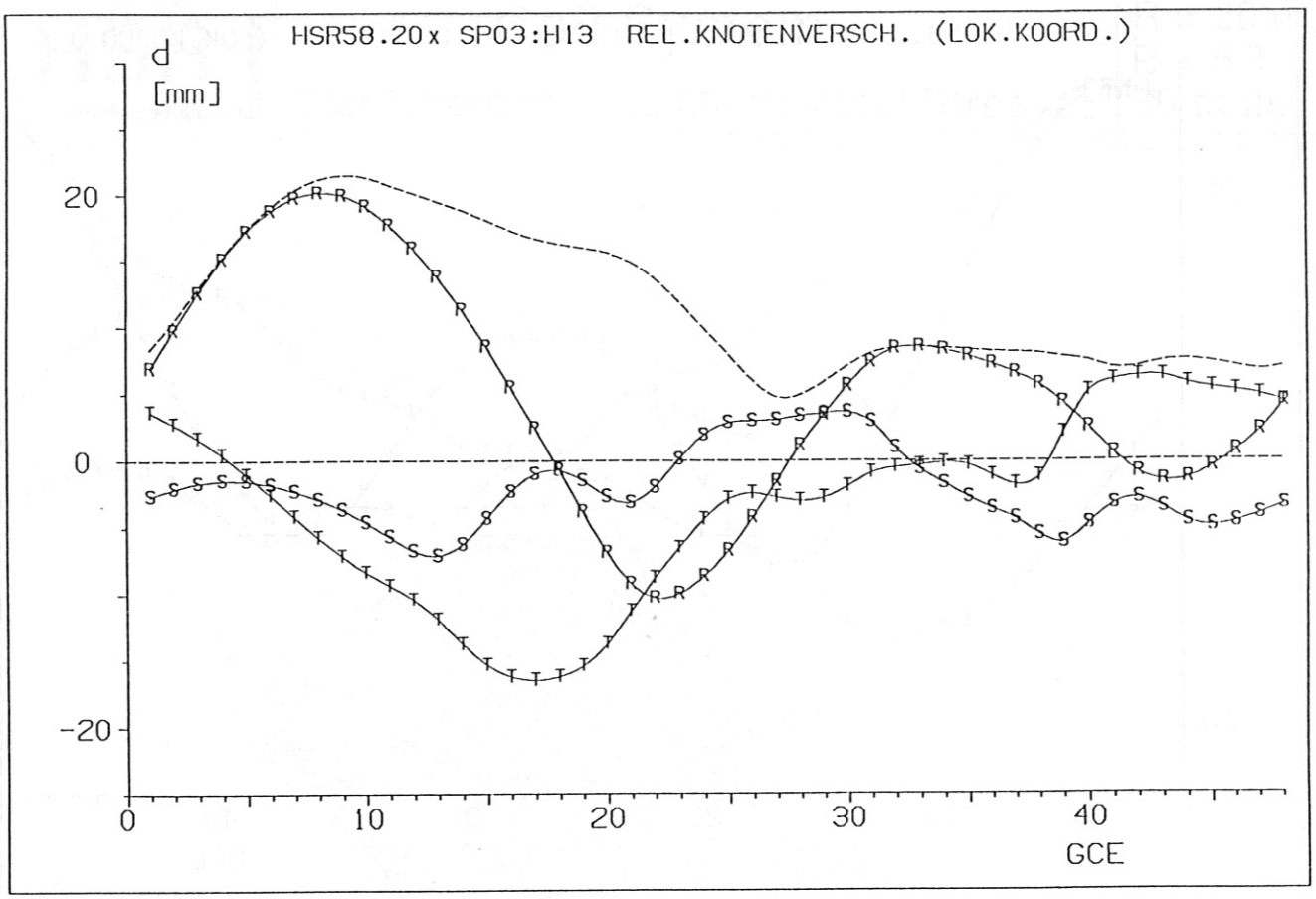

Fig. 5.15: HSR 5-8: Average displacement of coil 3 in radial, lateral and tangential direction.

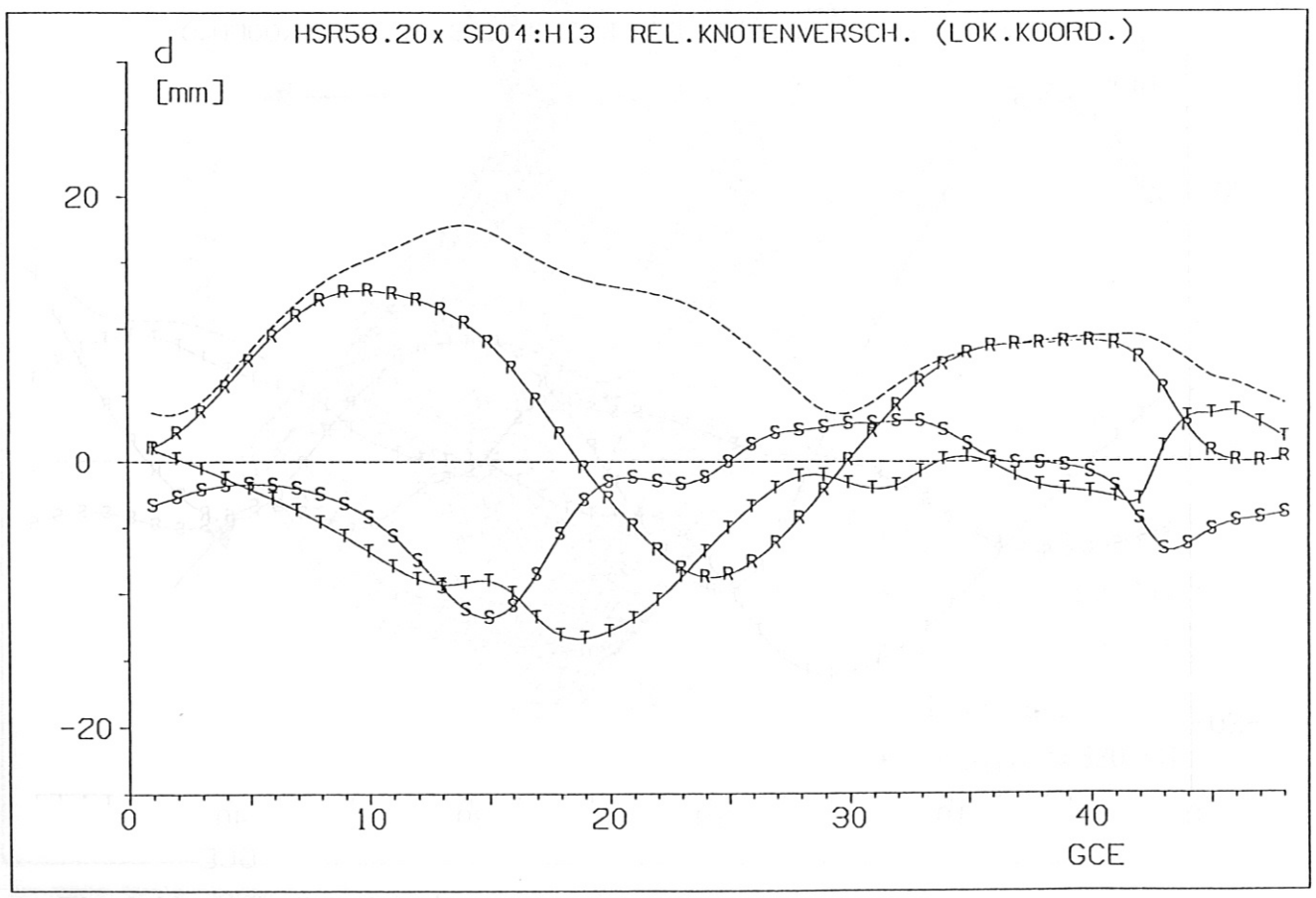

Fig. 5.16: as Fig. 5.15, for coil 4.

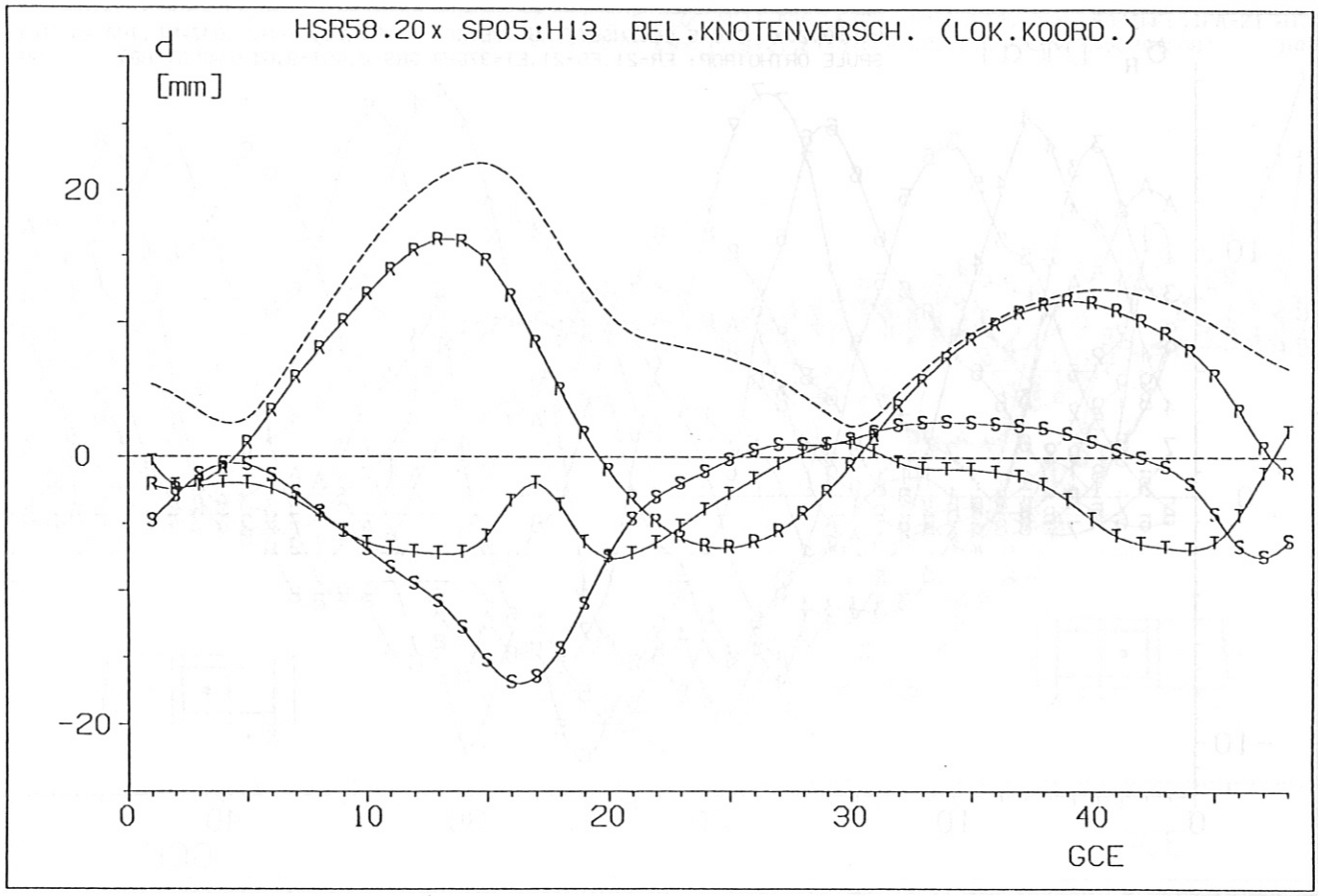

Fig. 5.17: HSR 5-8: Average displacement of coil 5 in radial, lateral and tangential direction.

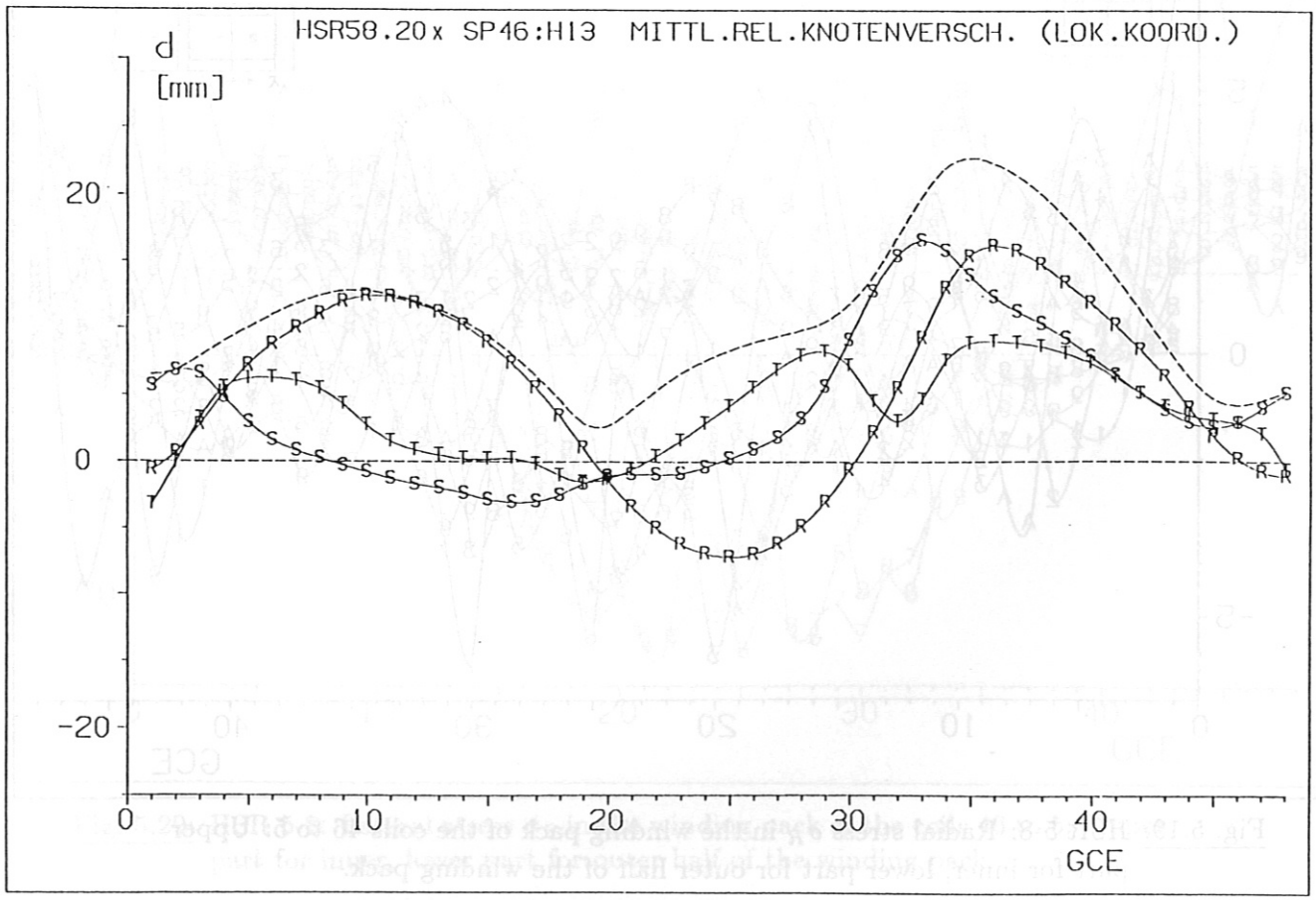

Fig. 5.18: HSR 5-8: Average displacement of coil 46 in radial, lateral and tangential direction. Coil 46 is antisymmetric to coil 5.

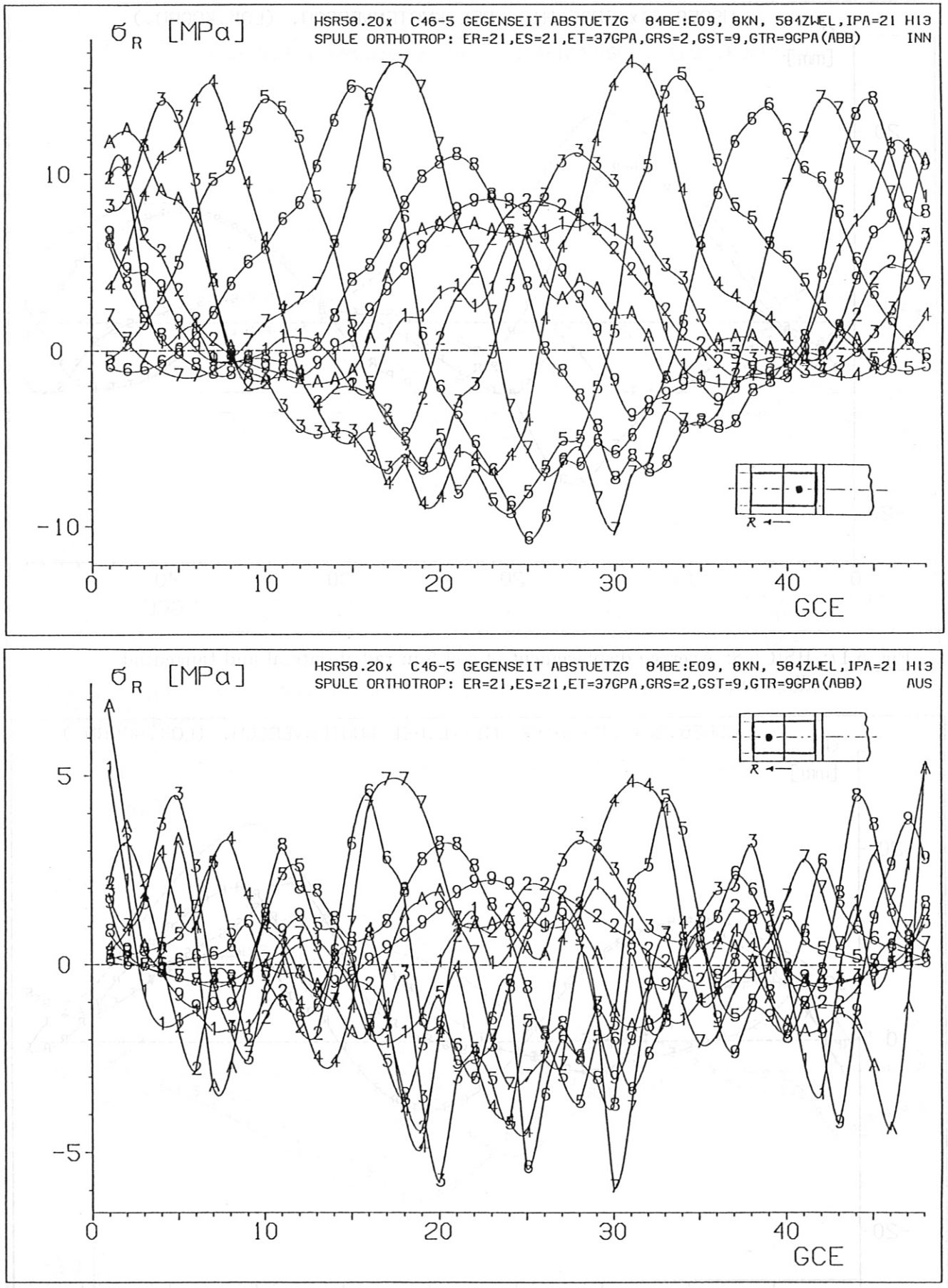

Fig. 5.19: HSR 5-8: Radial stress σ_R in the winding pack of the coils 46 to 5: Upper part for inner, lower part for outer half of the winding pack.

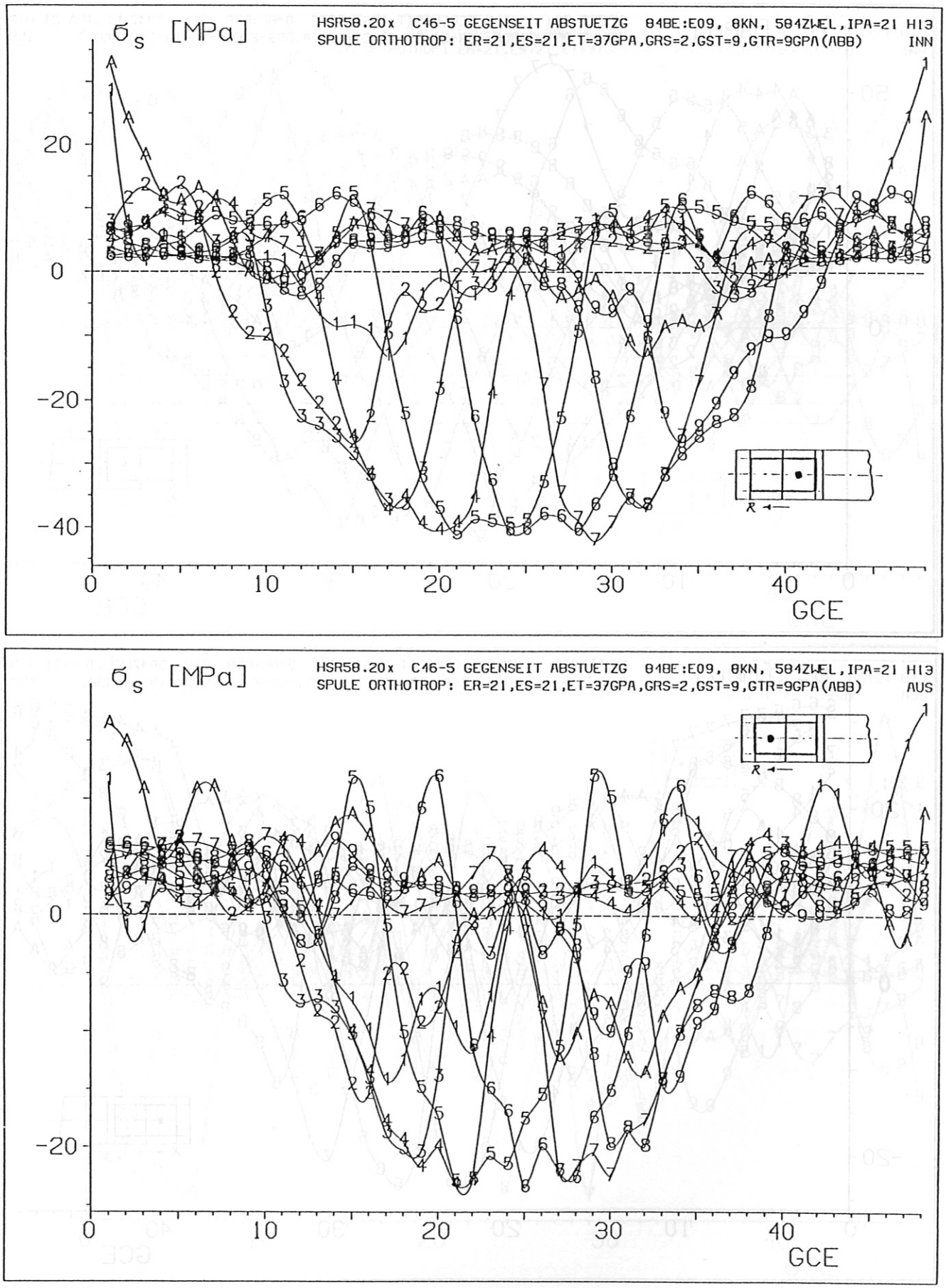

Fig. 5.20: HSR 5-8: Lateral stress σ_S in the winding pack of the coils 46 to 5: Upper part for inner, lower part for outer half of the winding pack.

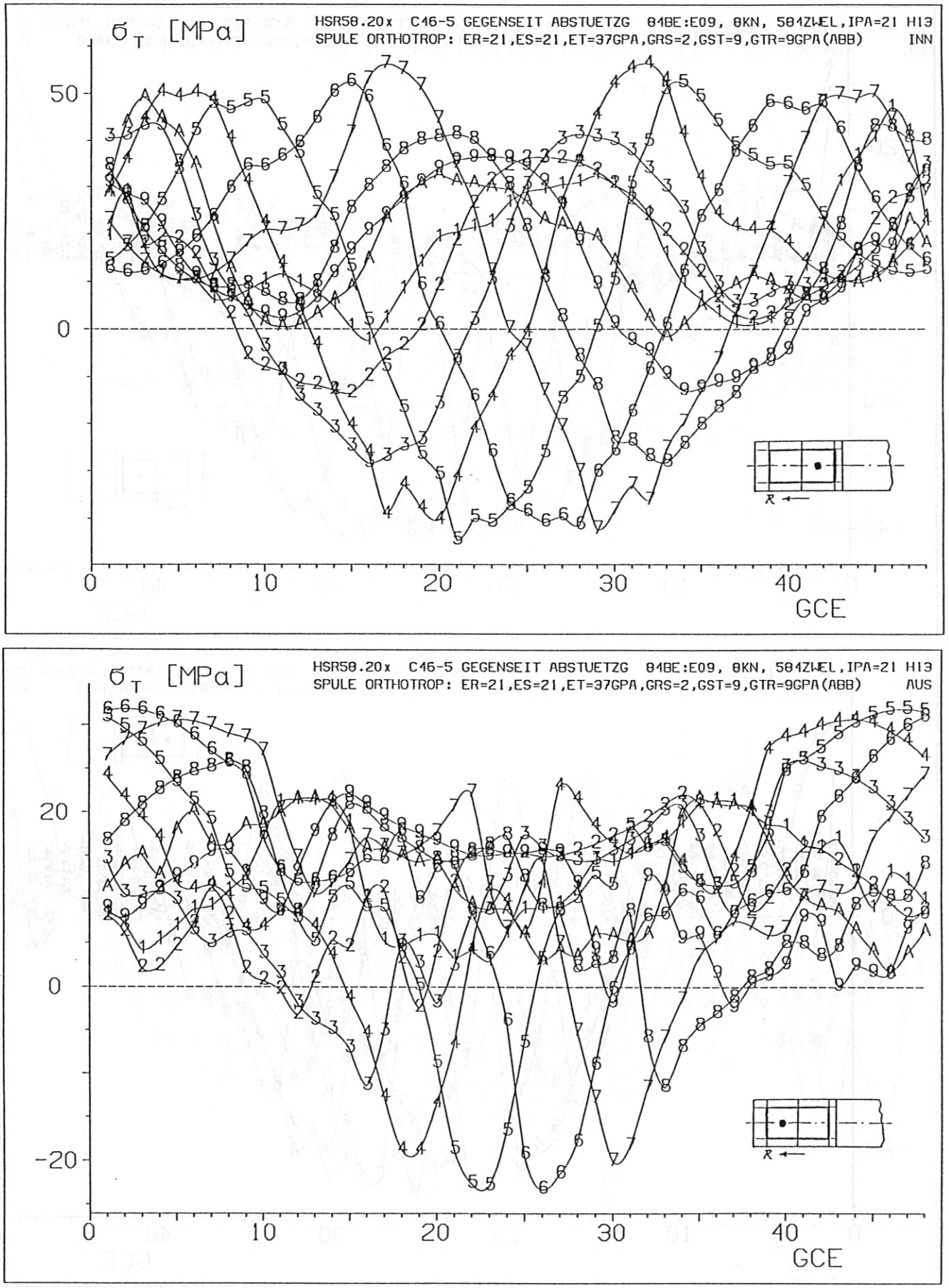

Fig. 5.21: HSR 5-8: Tangential stress σ_T in the winding pack of the coils 46 to 5: Upper part for inner, lower part for outer half of the winding pack.

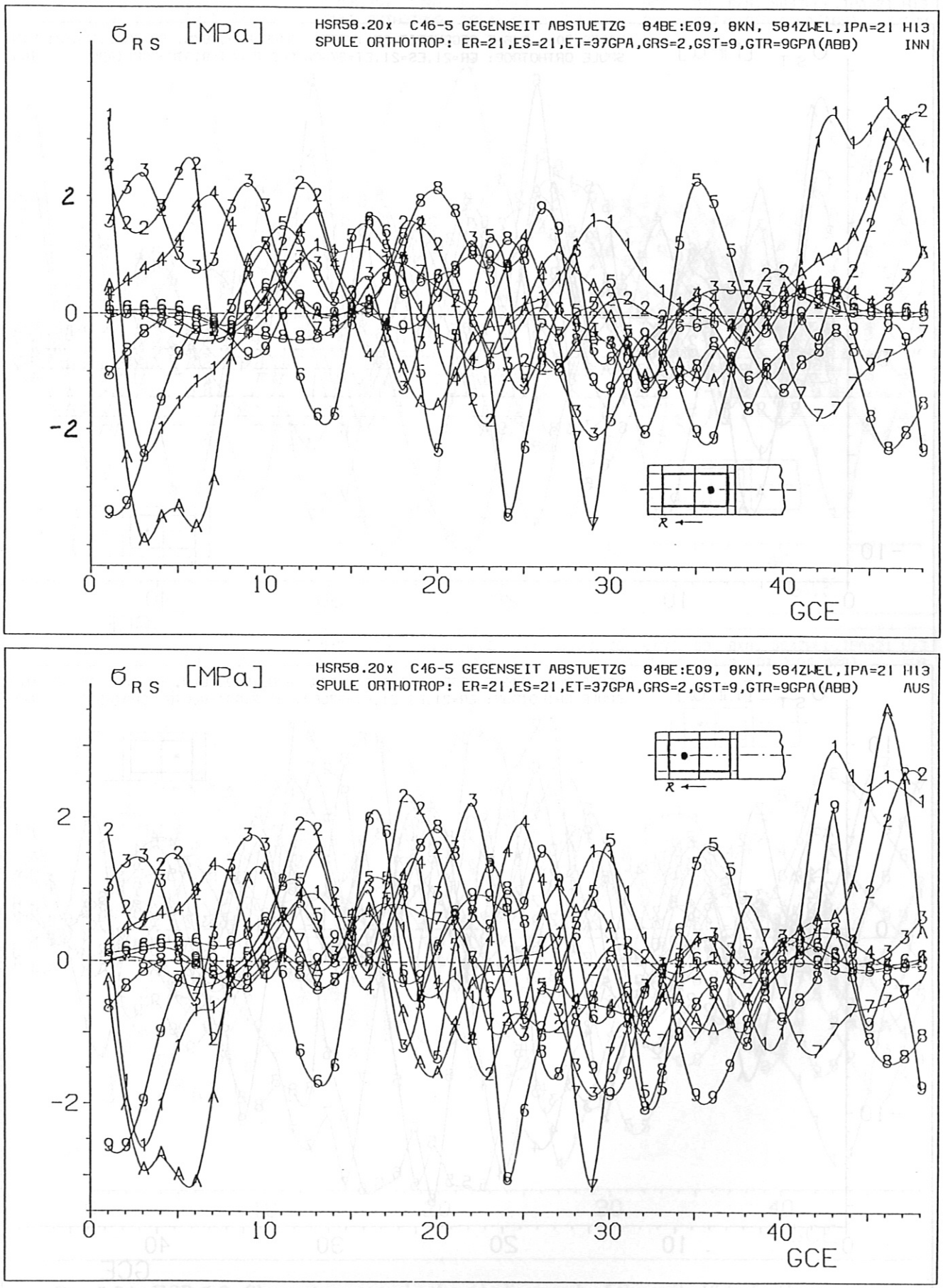

Fig. 5.22: HSR 5-8: Shear stress σ_{RS} in the winding pack of the coils 46 to 5: Upper part for inner, lower part for outer half of the winding pack.

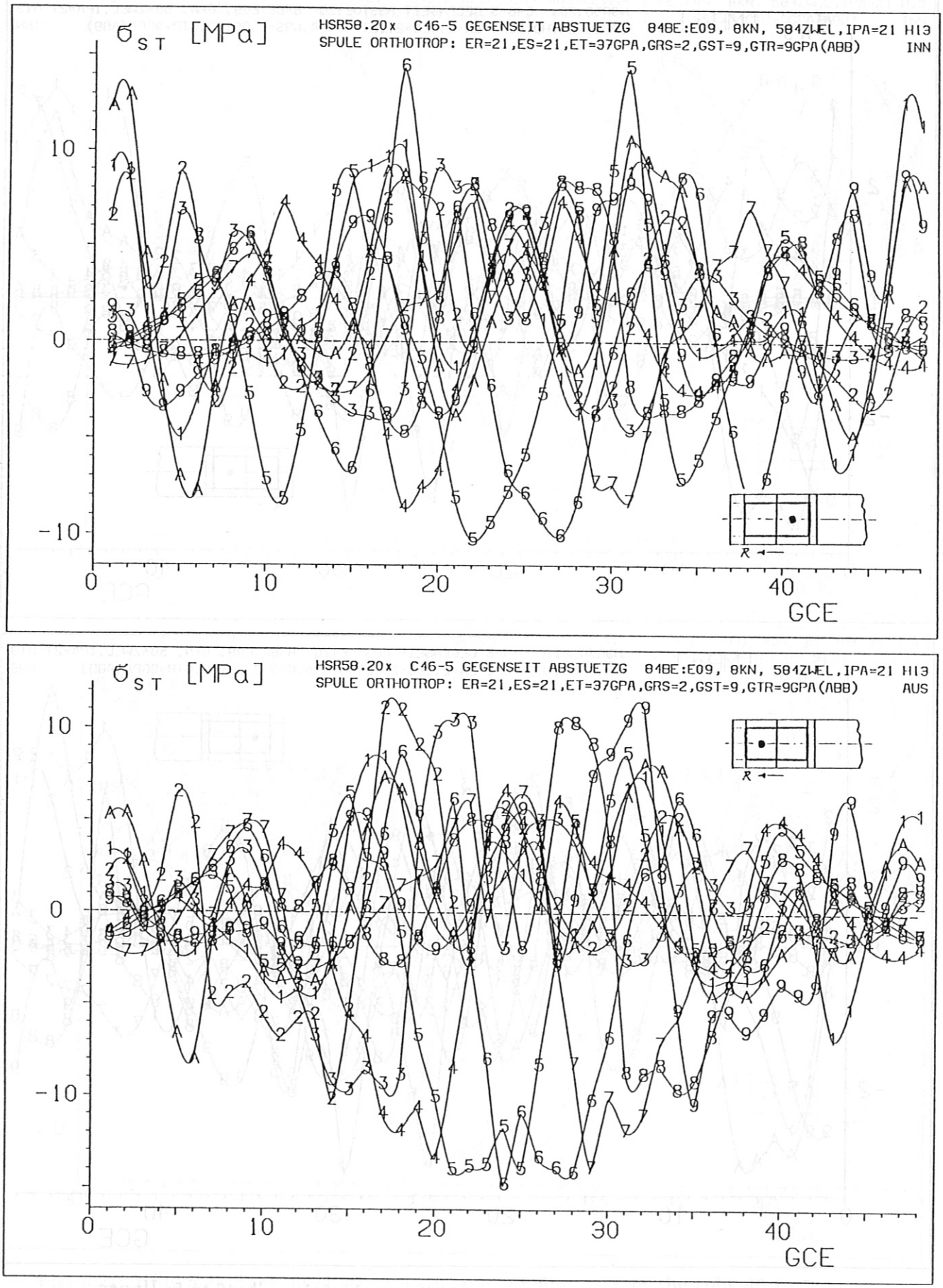

Fig. 5.23: HSR 5-8: Shear stress σ_{ST} in the winding pack of the coils 46 to 5: Upper part for inner, lower part for outer half of the winding pack.

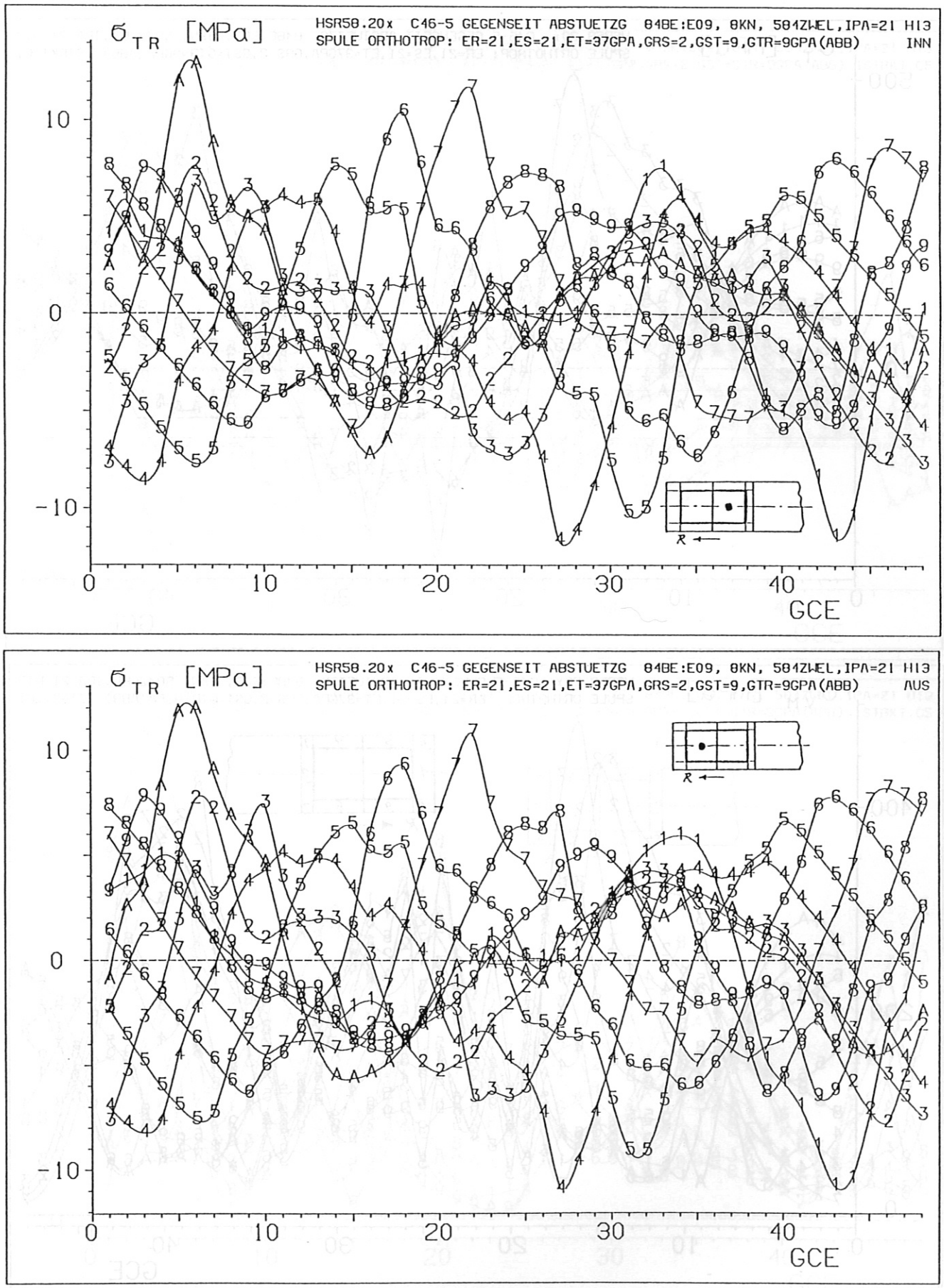

Fig. 5.24: HSR 5-8: Shear stress σ_{TR} in the winding pack of the coils 46 to 5: Upper part for inner, lower part for outer half of the winding pack.

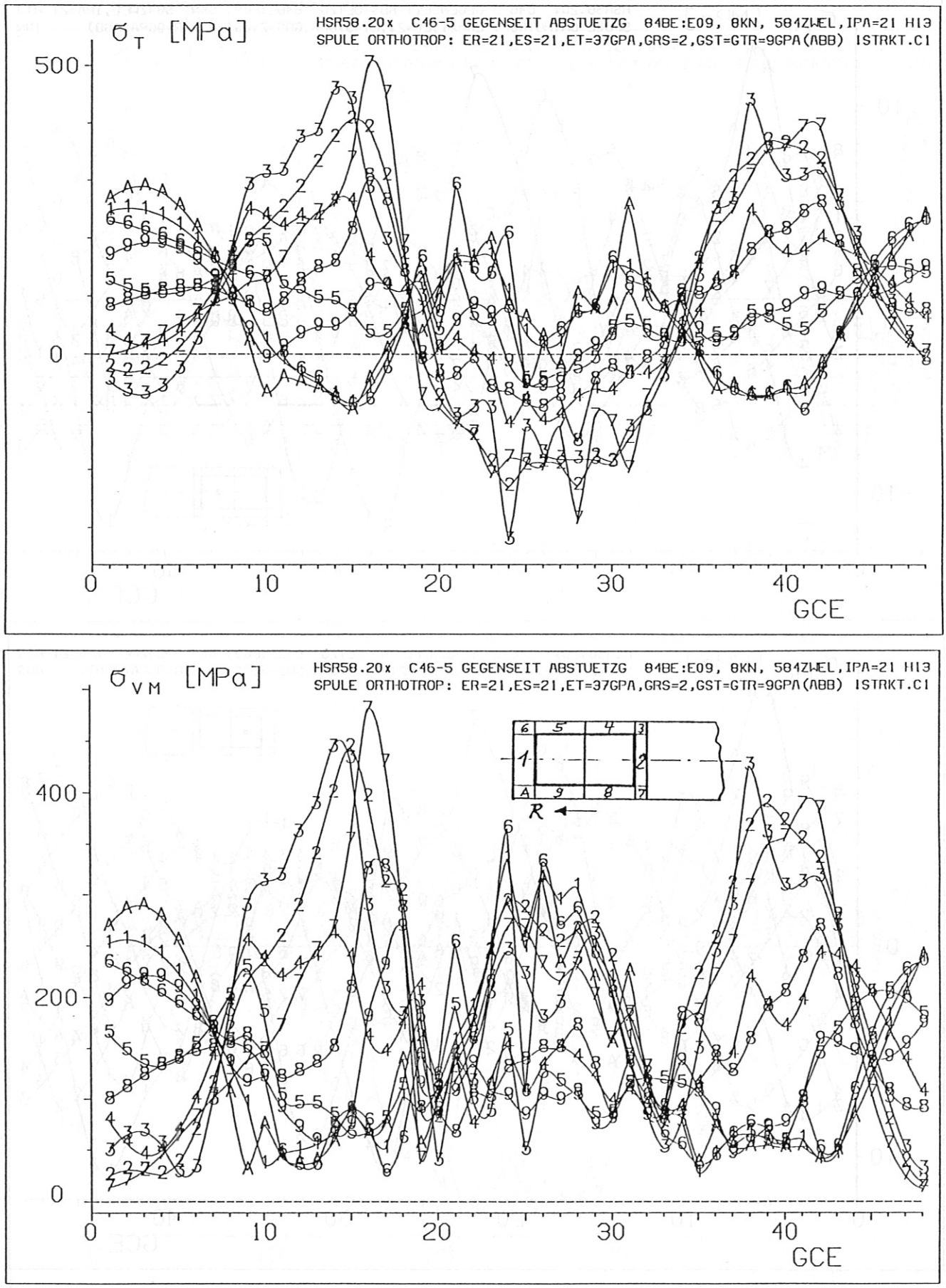

Fig. 5.25: Distribution of tangential stress σ_T and equivalent stress (von Mises stress) σ_{vM} for the coil housing of coil 1, see insert for position of elements.

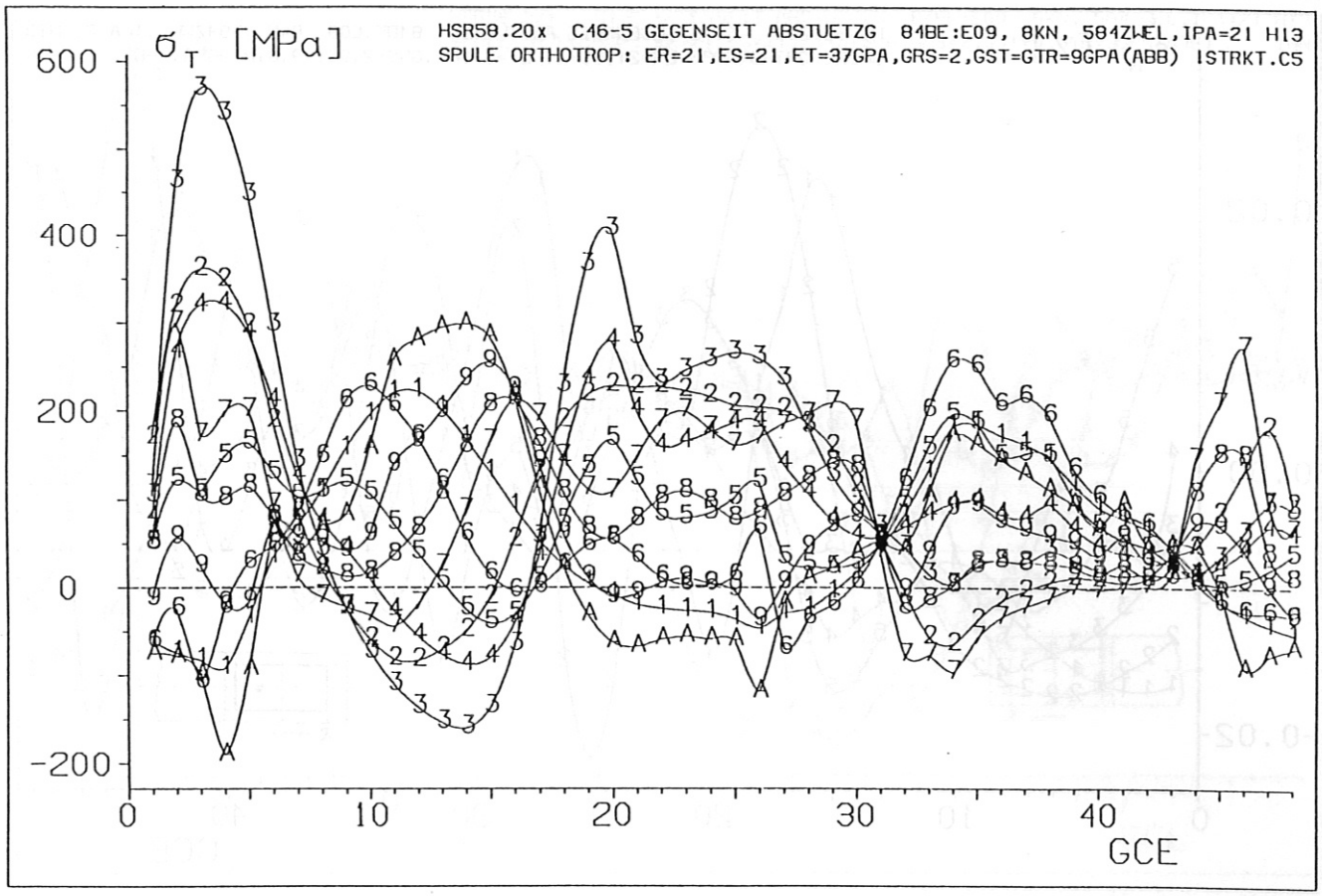

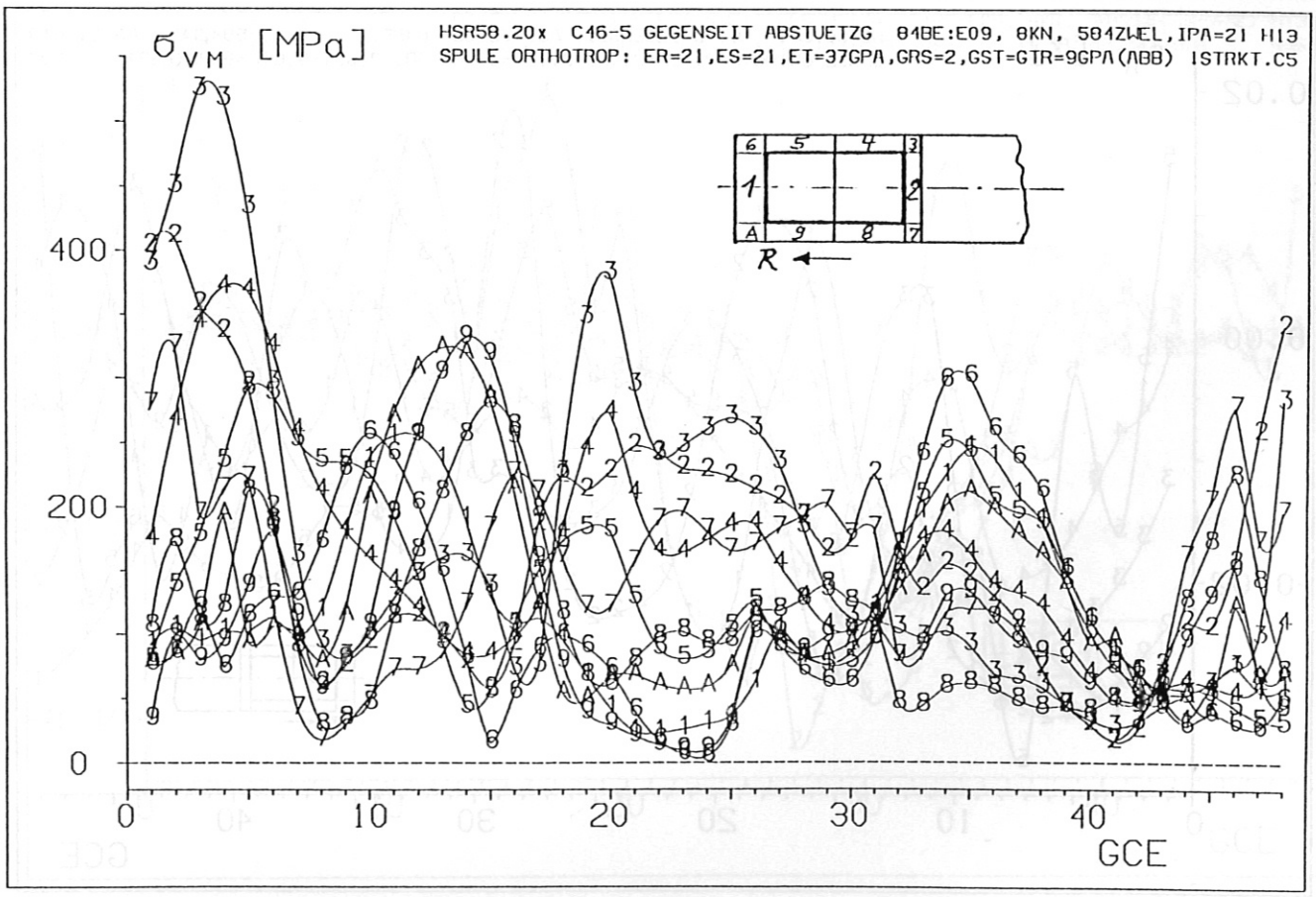

Fig. 5.26: Distribution of tangential stress σ_T and equivalent stress (von Mises stress) σ_{vM} for the coil housing of coil 5, see insert for position of element.

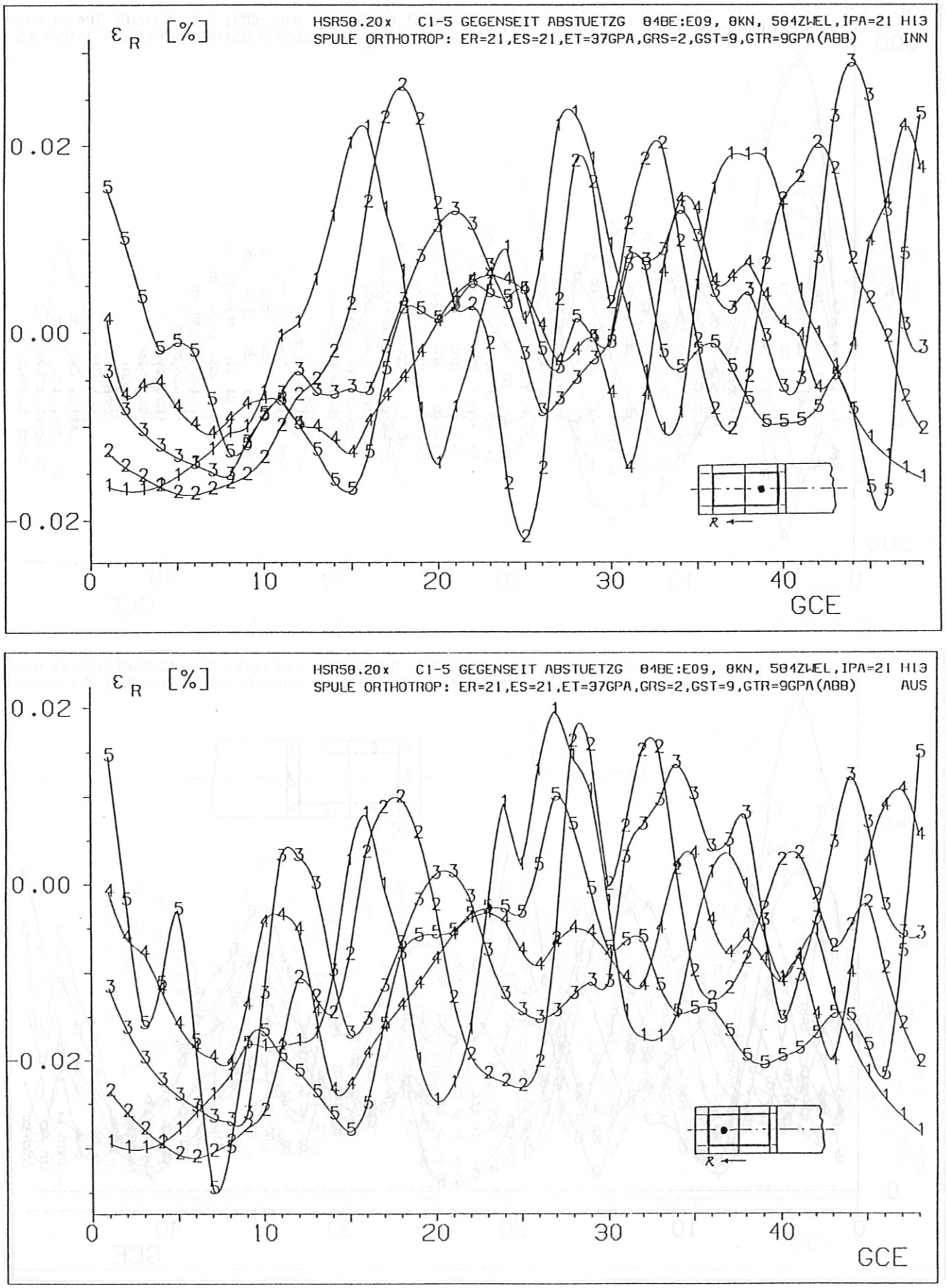

Fig. 5.27: HSR 5-8: Radial strain ε_R in the coil winding pack for the coils 1 to 5: Upper part for inner, lower part for outer half of the winding pack.

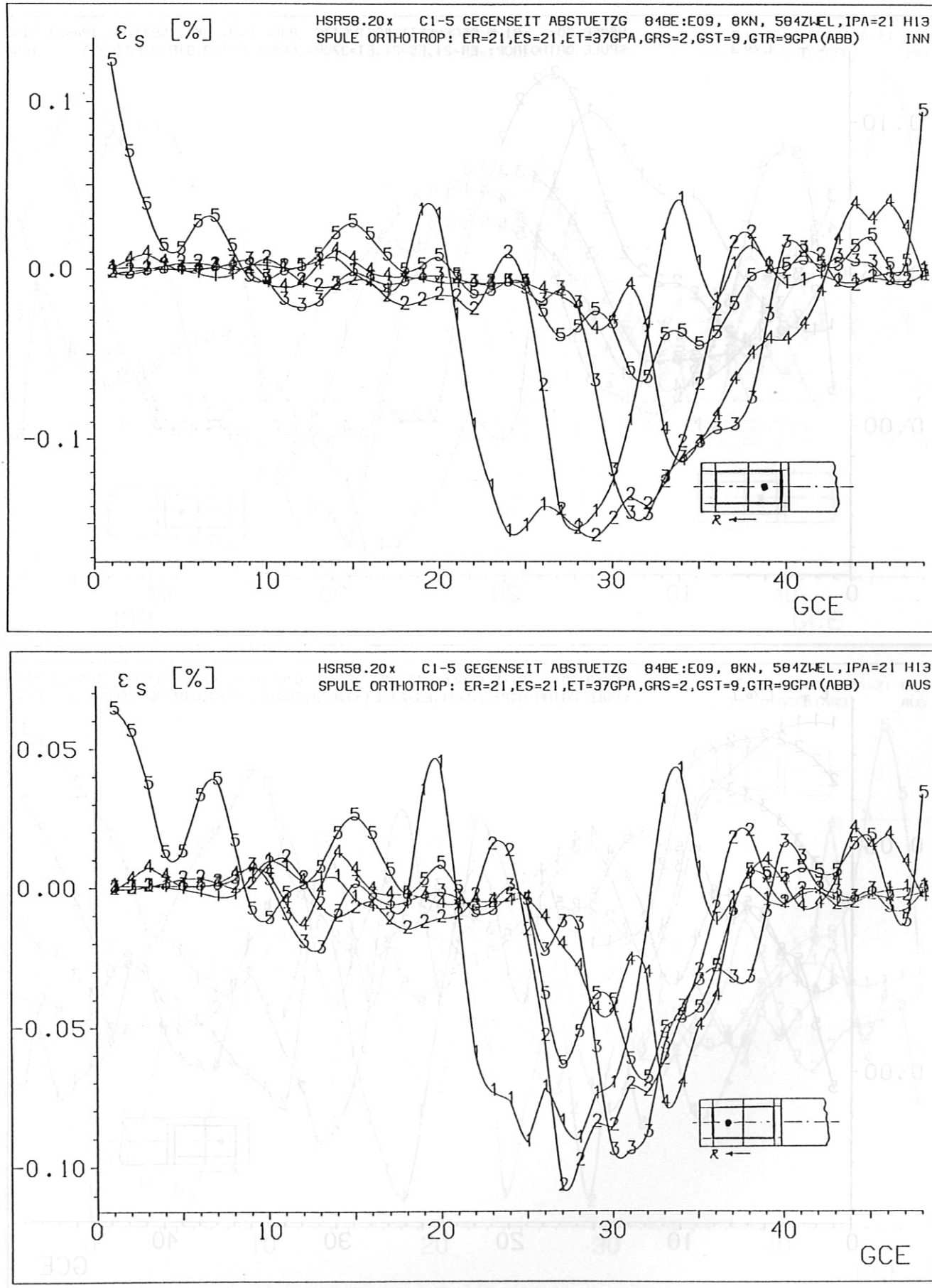

Fig. 5.28: HSR 5-8: Lateral strain ε_S in the coil winding pack for the coils 1 to 5: Upper part for inner, lower part for outer half of the winding pack.

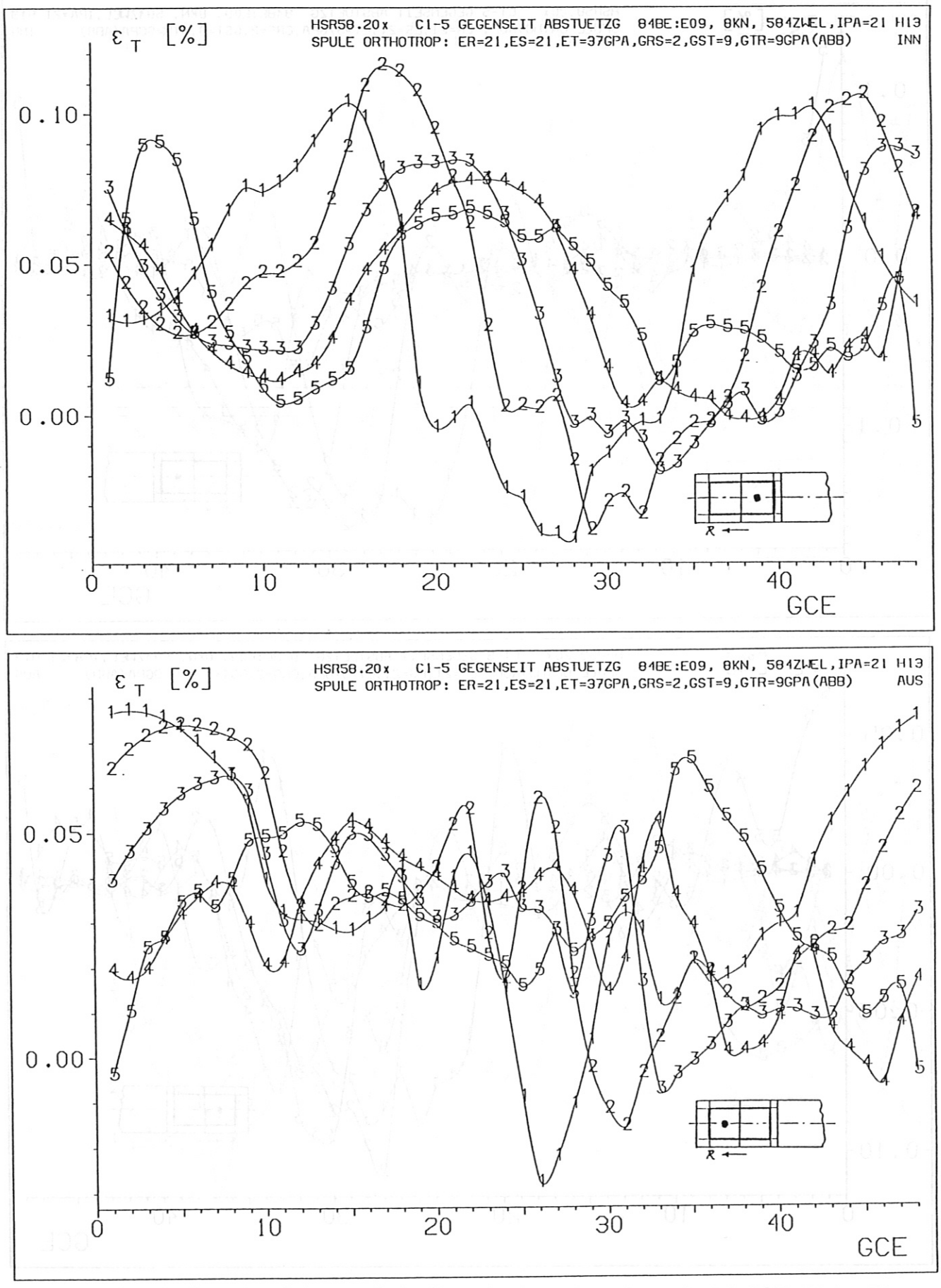

Fig. 5.29: HSR 5-8: Tangential strain ε_T in the coil winding pack for the coils 1 to 5: Upper part for inner, lower part for outer half of the winding pack.

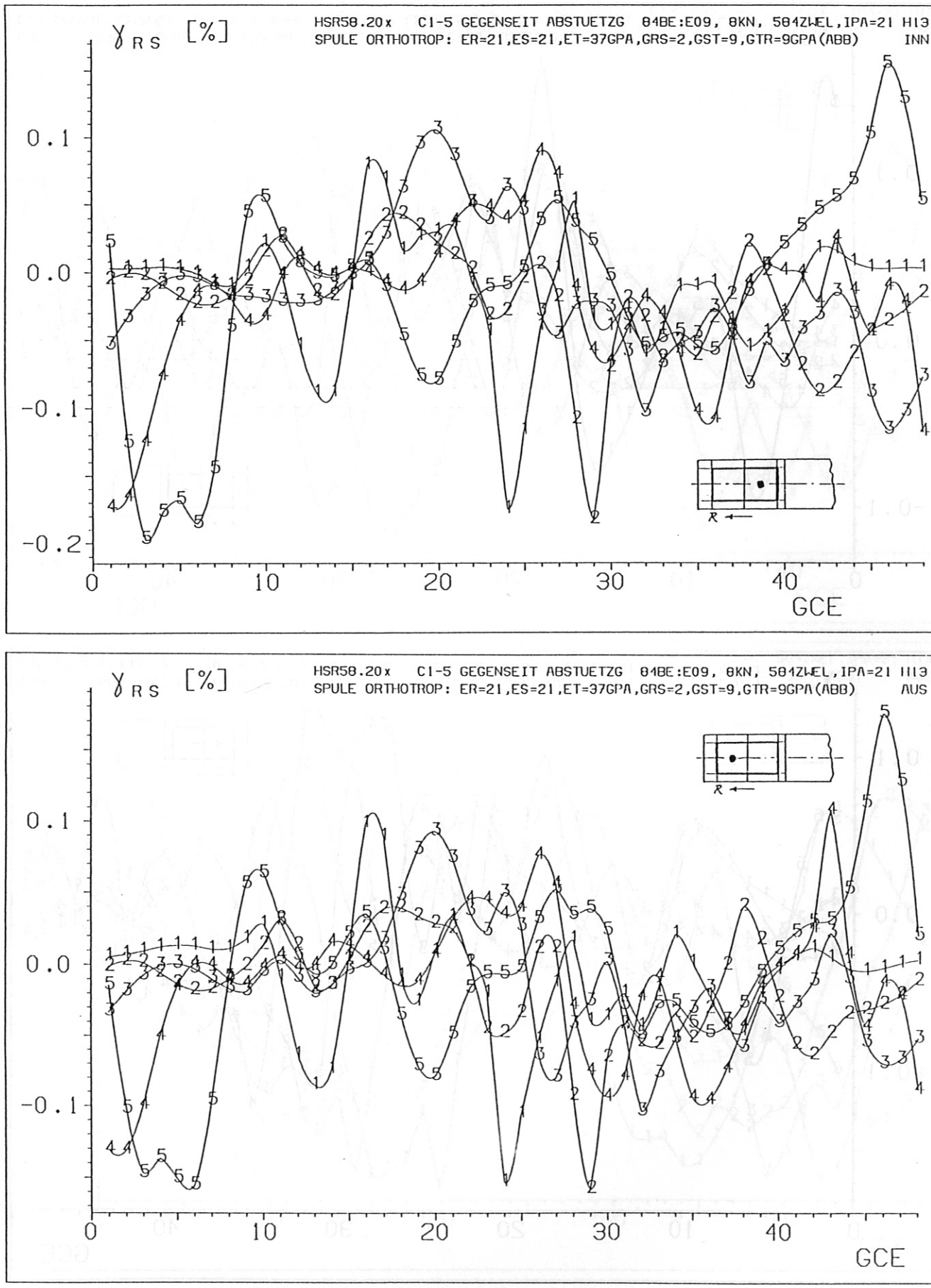

Fig. 5.30: HSR 5-8: Shear strain γ_{RS} in the coil winding pack for the coils 1 to 5: Upper part for inner, lower part for outer half of the winding pack.

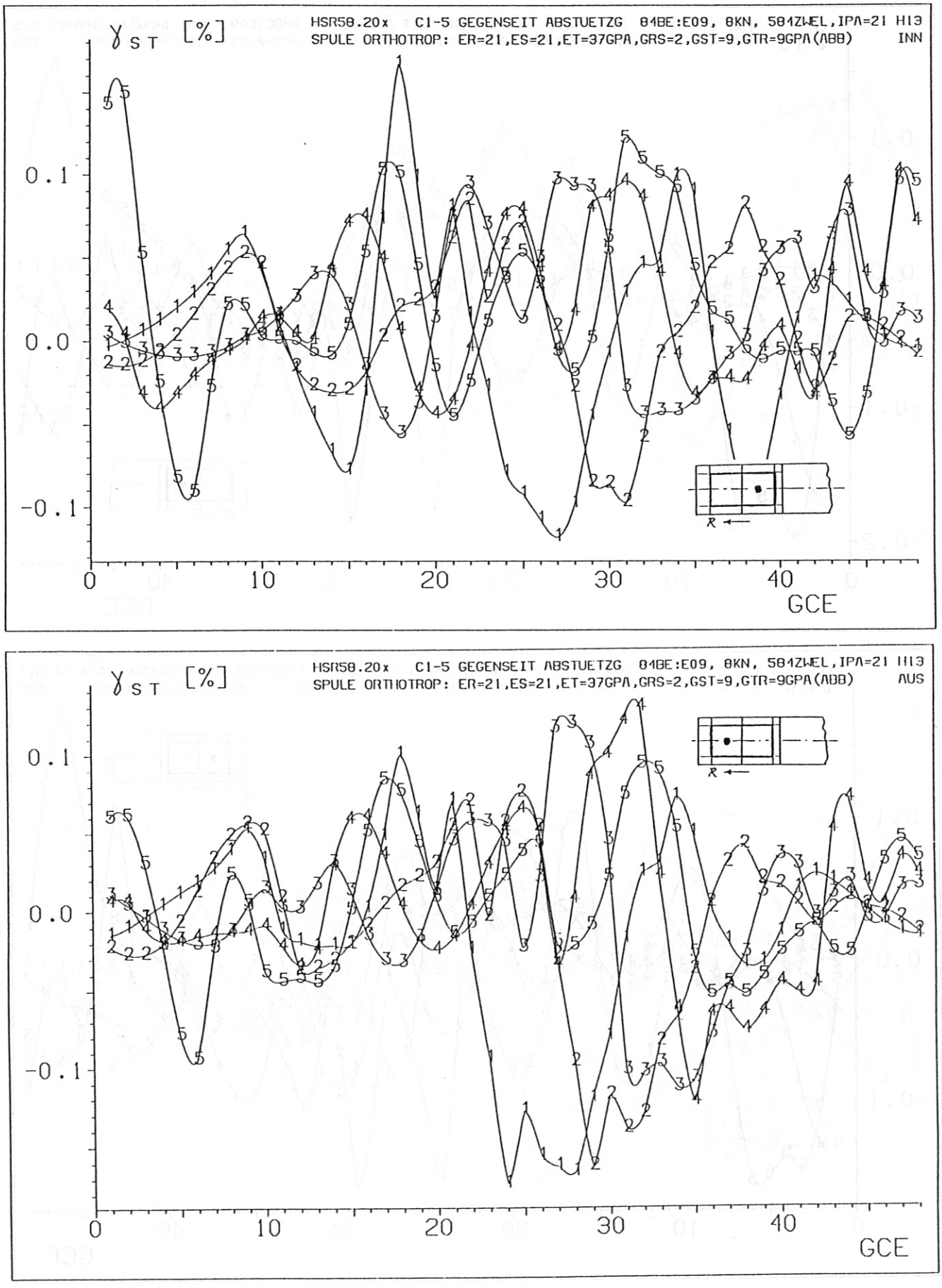

Fig. 5.31: HSR 5-8: Shear strain γ_{ST} in the coil winding pack for the coils 1 to 5: Upper part for inner, lower part for outer half of the winding pack.

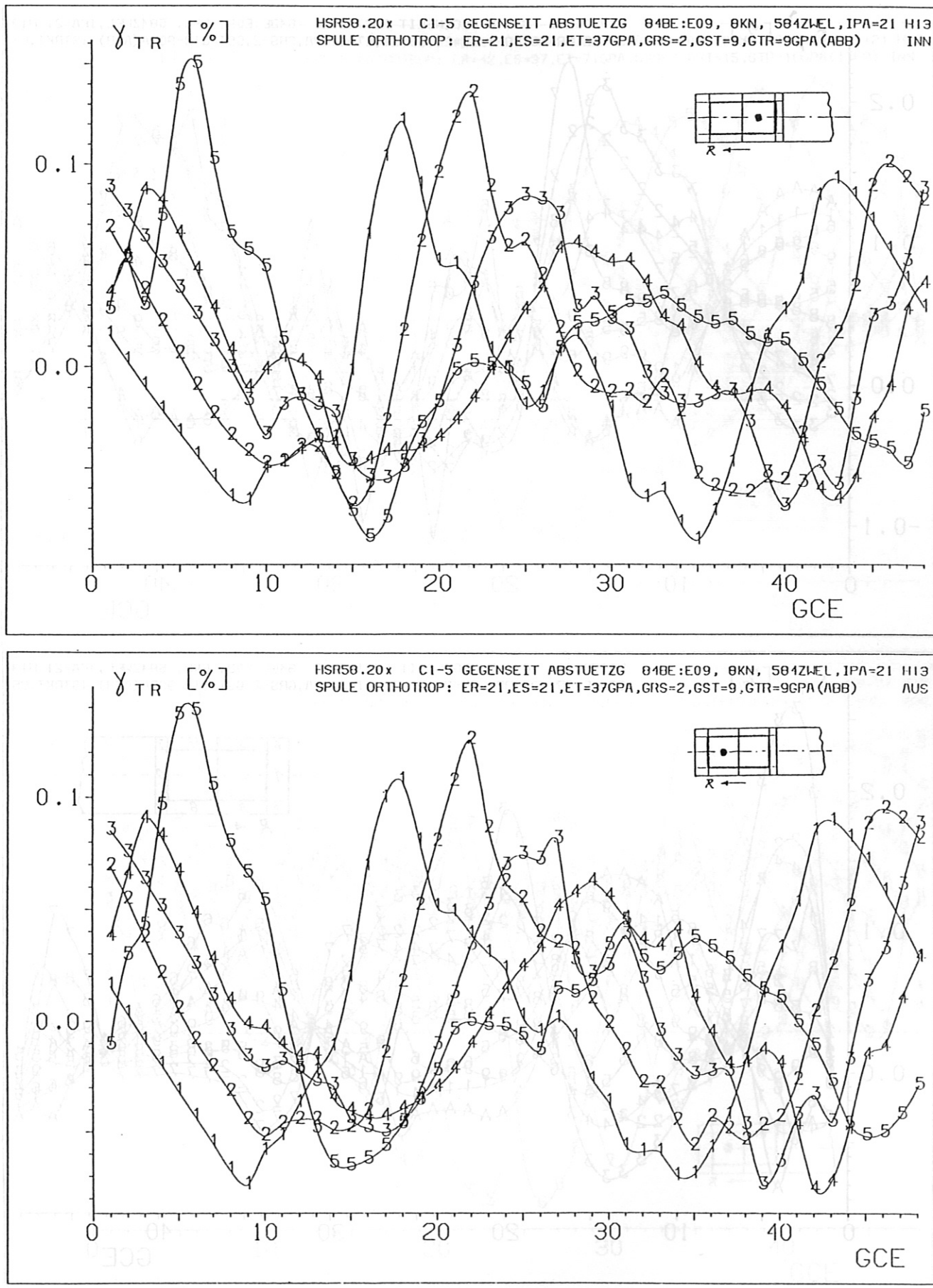

Fig. 5.32: HSR 5-8: Shear strain γ_{TR} in the coil winding pack for the coils 1 to 5: Upper part for inner, lower part for outer half of the winding pack.

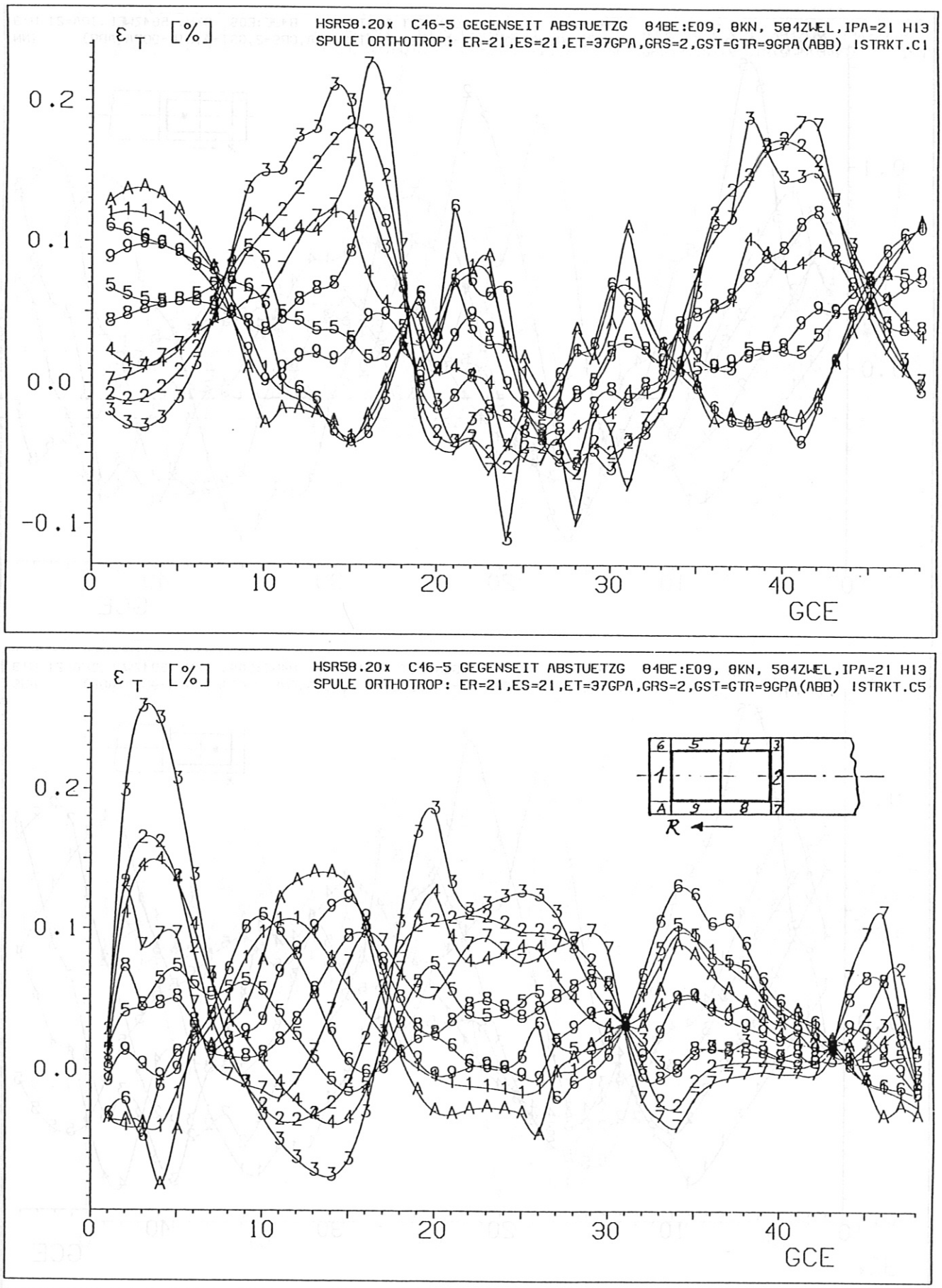

Fig. 5.33: HSR 5-8: Tangential strain ε_T for the coil housing of coil 1 (upper part) and coil 5 (lower part).

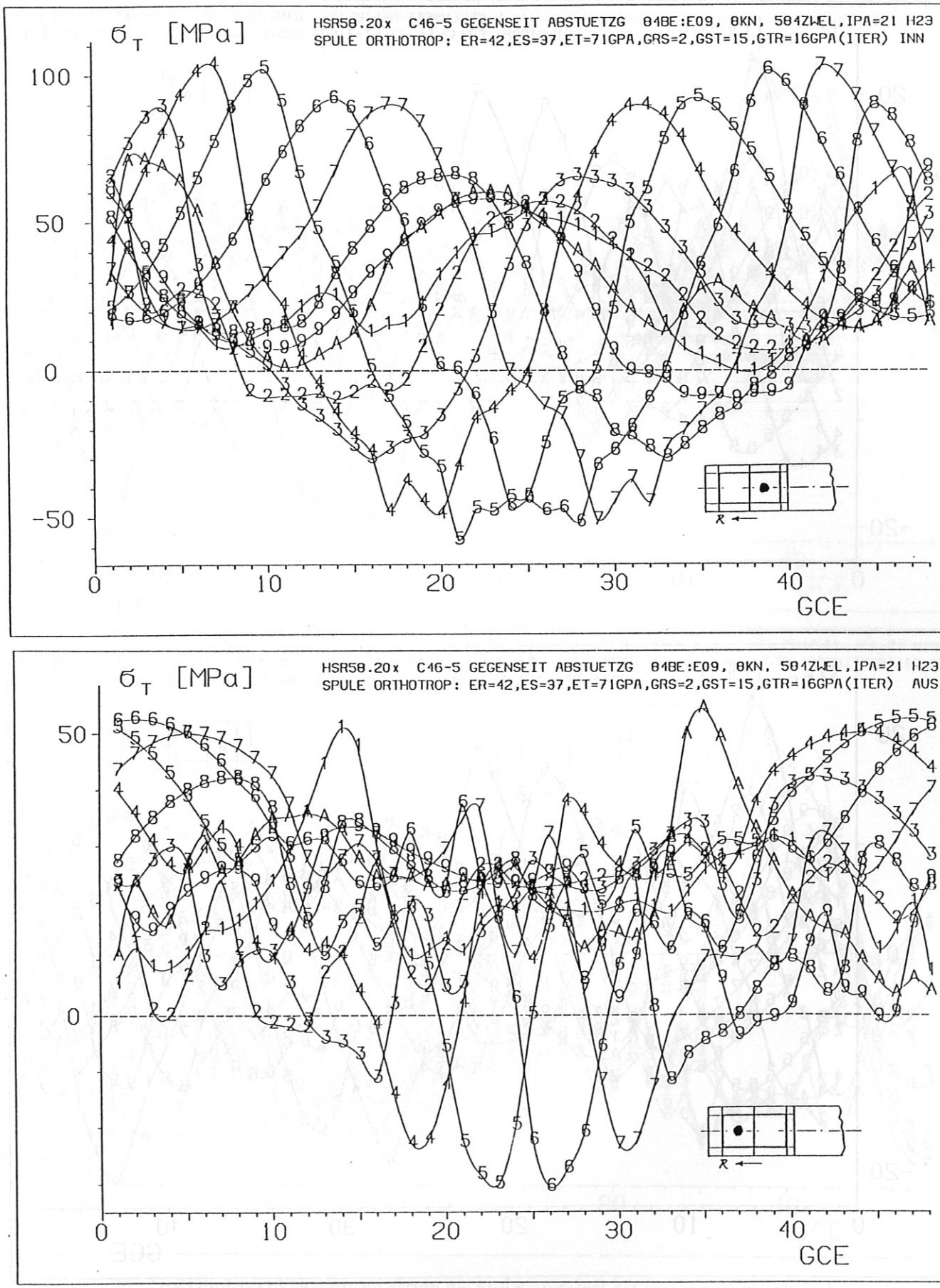

Fig. 5.34: HSR 5-8: Tangential stress σ_T in the winding pack of the coils 46 to 5: The elastic data of an ITER conductor is assumed. Upper part for inner, lower part for outer half of the winding pack.

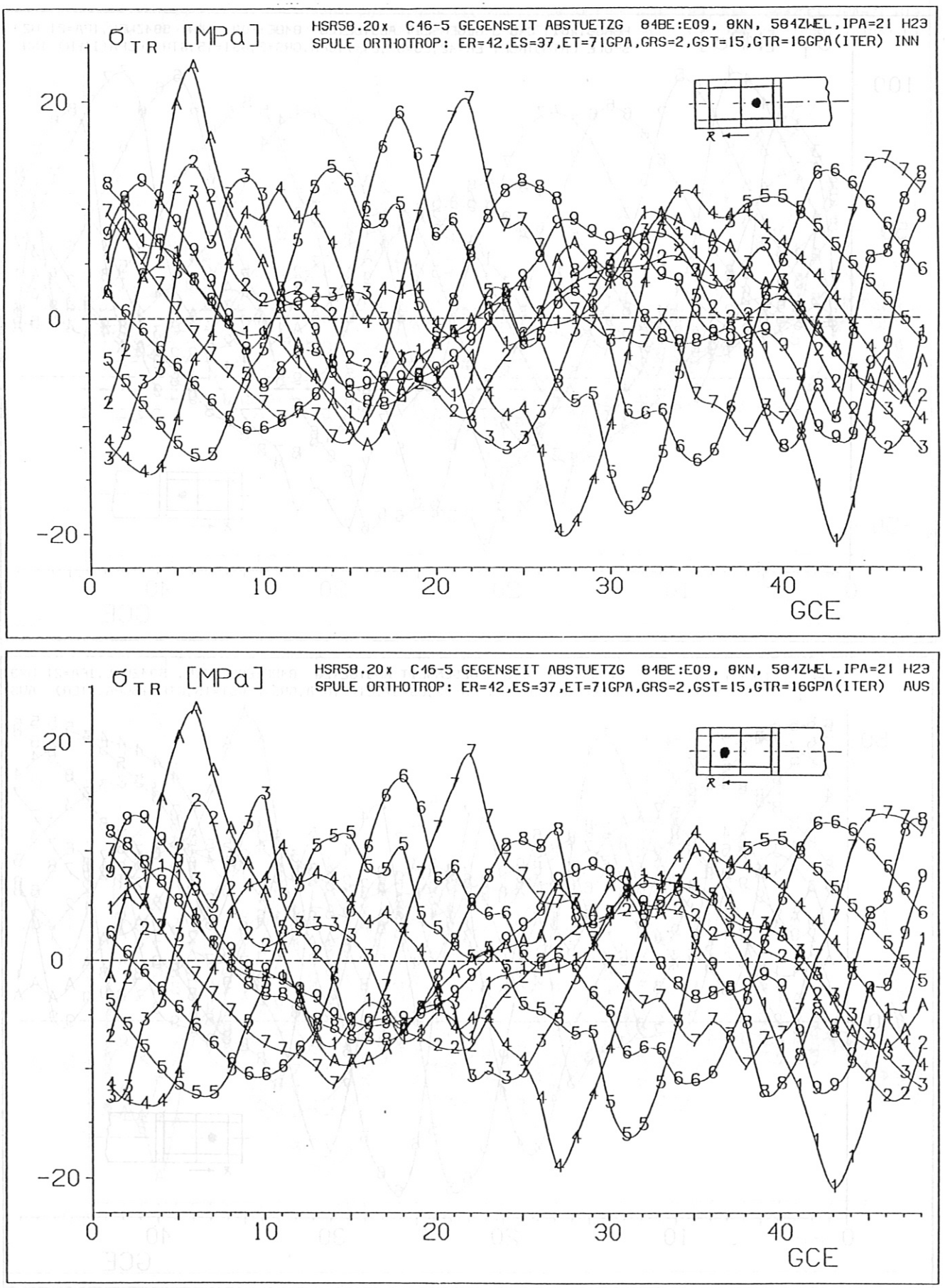

Fig. 5.35: HSR 5-8: Shear stress σ_{TR} in the winding pack of the coils 46 to 5: The elastic data of an ITER conductor is assumed. Upper part for inner, lower part for outer half of the winding pack.

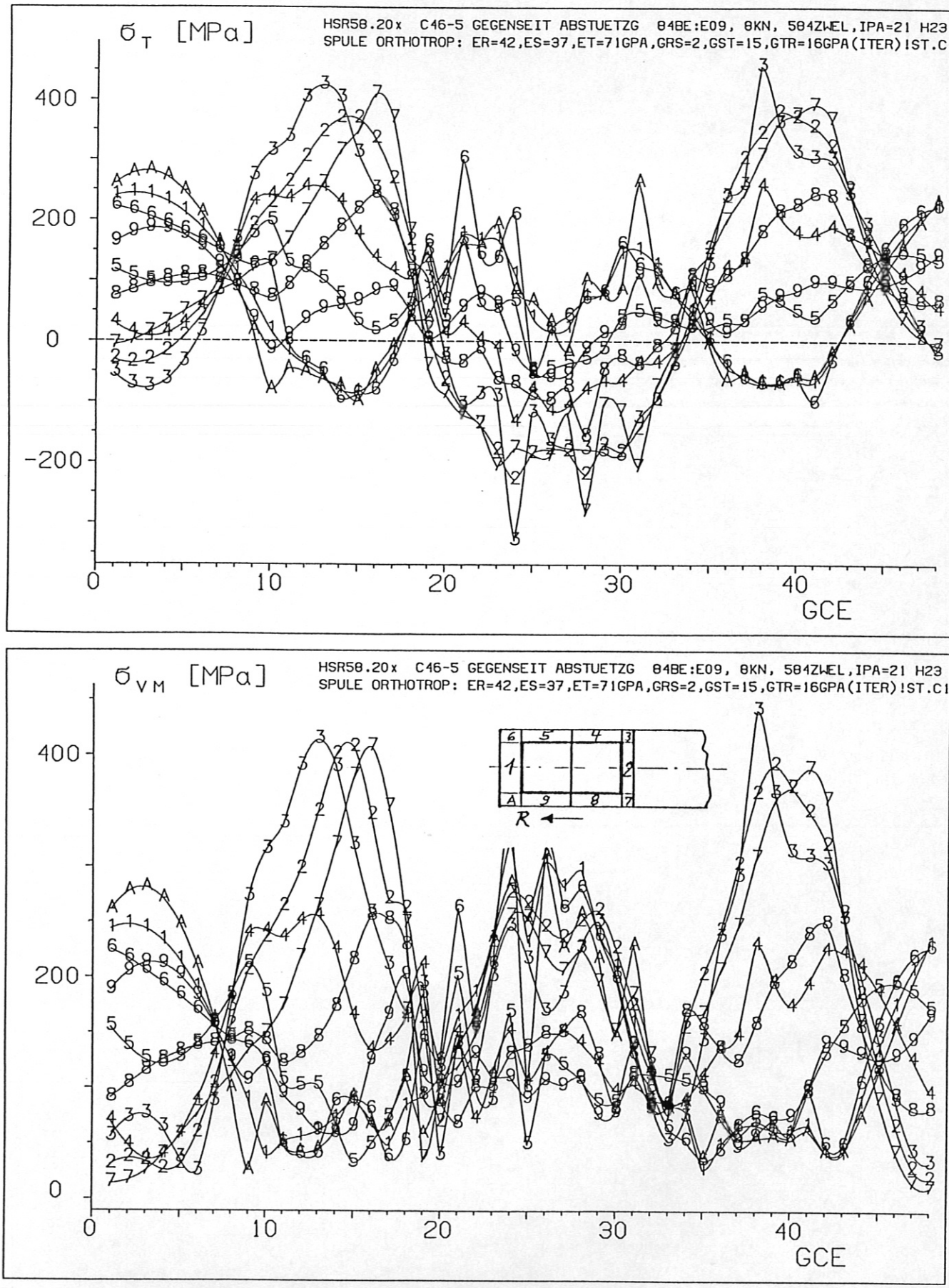

Fig. 5.36: Distribution of tangential stress σ_T and equivalent stress (von Mises stress) σ_{vM} for the coil housing of coil 1, see insert for position of elements. The elastic data of an ITER conductor is assumed.